minerals

MDPI

Article

Petrogenesis and Tectonic Implications of the Cryogenian I-Type Granodiorites from Gabgaba Terrane (NE Sudan)

Mabrouk Sami [1], Munir M. A. Adam [2,*], Xinbiao Lv [2,3], El Saeed R. Lasheen [4], Antoaneta Ene [5,*], Hesham M. H. Zakaly [6,7,*], Saad S. Alarifi [8], Nasser M. Mahdy [9], Abdel Rahman A. Abdel Rahman [10], Adil Saeed [10], Esam S. Farahat [1], Douaa Fathy [1] and Shehata Ali [1]

1 Geology Department, Faculty of Science, Minia University, El-Minia 61519, Egypt
2 Faculty of Earth Resources, China University of Geosciences, Wuhan 430074, China
3 Geological Survey, Faculty of Earth Resources, China University of Geosciences, Wuhan 430074, China
4 Geology Department, Faculty of Science, Al-Azhar University, Cairo 11884, Egypt
5 INPOLDE Research Center, Department of Chemistry, Physics and Environment, Faculty of Sciences and Environment, Dunarea de Jos University of Galati, 800008 Galati, Romania
6 Institute of Physics and Technology, Ural Federal University, Yekaterinburg 620002, Russia
7 Physics Department, Faculty of Science, Al-Azhar University, Assiut 71524, Egypt
8 Department of Geology and Geophysics, College of Science, King Saud University, P.O. Box 2455, Riyadh 11451, Saudi Arabia
9 Nuclear Materials Authority, El-Maadi, Cairo 11381, Egypt
10 College of Petroleum Geology and Minerals, University of Bahri, Khartoum North 11116, Sudan
* Correspondence: munirkonil@hotmail.com (M.M.A.A.); antoaneta.ene@ugal.ro (A.E.); h.m.zakaly@azhar.edu.eg (H.M.H.Z.)

Abstract: The widely distributed granitic intrusions in the Nubian Shield can provide comprehensive data for understanding its crustal evolution. We present new bulk-rock geochemistry and isotopic (zircon U-Pb and Lu-Hf) data from the Haweit granodiorites in the Gabgaba Terrane (NE Sudan). The dated zircons presented a $^{206}Pb/^{238}U$ Concordia age of 718.5 ± 2.2 Ma, indicating that they crystallized during the Cryogenian. The granodiorites contain both biotite and amphibole as the main mafic constituents. The samples exhibit metaluminous (A/CNK = 0.84–0.94) and calc-alkaline signatures. Their mineralogical composition and remarkable low P_2O_5, Zr, Ce, and Nb concentrations confirm that they belong to I-type granites. They exhibit subduction-related magma geochemical characters such as enrichment in LILEs and LREEs and depletion in HFSEs and HREEs, with a low $(La/Yb)_N$ ratio (3.0–5.9) and apparent negative Nb anomaly. The positive Hf(t) values (+7.34 to +11.21) and young crustal model age (T_{DM}^{C} = 734–985 Ma) indicates a juvenile composition of the granodiorites. The data suggest that the Haweit granodiorites may have formed from partially melting a juvenile low-K mafic source. During subduction, the ascending asthenosphere melts might heat and partially melt the pre-existing lower crust mafic materials to generate the Haweit granodiorites in the middle segment of the Nubian Shield.

Keywords: I-type granite; zircon U-Pb-Lu-Hf isotopes; Cryogenian; partial melting; Gabgaba Terrane; NE Sudan

Citation: Sami, M.; Adam, M.M.A.; Lv, X.; Lasheen, E.S.R.; Ene, A.; Zakaly, H.M.H.; Alarifi, S.S.; Mahdy, N.M.; Abdel Rahman, A.R.A.; Saeed, A.; et al. Petrogenesis and Tectonic Implications of the Cryogenian I-Type Granodiorites from Gabgaba Terrane (NE Sudan). *Minerals* **2023**, *13*, 331. https://doi.org/10.3390/min13030331

Academic Editors: Shuang-Qing Li and Long Chen

Received: 23 January 2023
Revised: 21 February 2023
Accepted: 23 February 2023
Published: 27 February 2023

1. Introduction

Granitic rocks have been observed in a variety of tectonic settings and are frequently linked to the beginning and end of supercontinent cycles [1–4]. I-type granites, the most common forms of continental granites, provide an important window into variable crust-mantle magmatic processes [5]. They were mostly generated from mantle and/or crustal sources and juvenile to ancient crystalline rocks [6–8]. Additionally, a variety of magmatic operations, including magma mixing, fractional crystallization, and partial melting [9], entrainment of peritectic assemblages [10], and different types of source rocks [11], may all have an impact on the geochemical properties of these rocks. Therefore, understanding the

petrogenesis and geochemical variability of I-type granites is critical for monitoring the crustal evolution of different orogenic belts.

The Arabian–Nubian Shield (ANS) Neoproterozoic terrains, including the Sudanese basement complex, are important archives of one of Earth's most tremendous geological episodes [12]. The juvenile ANS accretionary belt hosts a group of Neoproterozoic (950–550 Ma) arc terranes (Figure 1A) that were formed and amalgamated by numerous significant tectono-magmatic episodes throughout the prolonged East African Orogeny [3,13,14]. The sequence of the ANS formation begins with the creation of oceanic arcs and the formation of collisional and post-collisional magmatic bodies (~630–550 Ma). The East African orogeny significantly modified the internal structure of the ANS and led to the formation of several terranes separated by major faults and suture zones (Figure 1A).

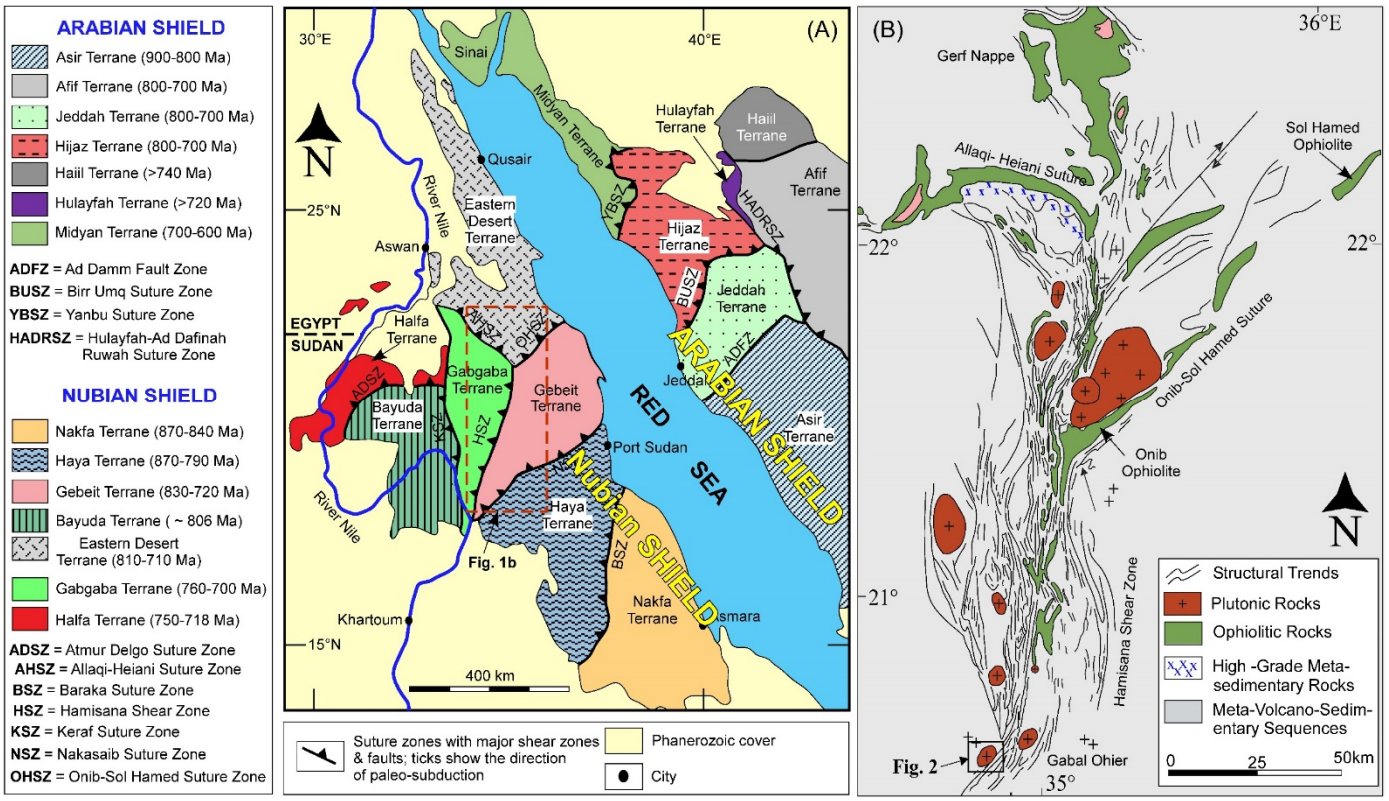

Figure 1. (**A**) The ANS geological and structural map [13,15] shows tectonostratigraphic terranes with estimated terrane protolith ages, as well as subduction directions, suture zones, and boundaries between the ANS and bordering older crustal blocks. The dashed line red rectangular is the HSZ, marked as b: (**B**) general geologic map of the plexus, including the eastern part of the Gerf nappe, the Onib–Sol Hamed suture, the Allaqi–Heiani suture, and the HSZ [16]. The structural trends represent field structural data measured by Stern et al. [16] and they represent a combination of low angle thrust fault, deformations, dextral shears, and folded structures.

The ANS, due to its juvenile character and widespread occurrence, provides an ideal natural environment for understanding the crustal evolution (timing, magma source, and petrogenesis) of various magmatic rocks in general and granitic rocks in particular. Many studies, based on precious geochemical and geochronological data, improve our knowledge about the nature of the ANS crystalline rocks [4,17–22]. Although several recent studies on some Sudanese crystalline rocks have been conducted [13,23–26], they still need further investigation and documentation, and their relative inaccessibility remains a crucial research challenge.

In NE Sudan, the Hamisana Shear Zone (HSZ) represents a zone of deformation that extends for ~300 km along strike and about 50 km in width between the Gabgaba

and Gebeit terranes (Figure 1A). Different types of granitoids (e.g., granite, syenite, granodiorite, quartz monzonite, and tonalite) are widely occurring in the Gabgaba Terrane (Figure 1B), and some of them are economically interesting due to the associated gold mineralization [24]. Little information is known about the evolution, tectonic setting, source of magma, and crystallization age of these granitoids, especially those that occupied the southern parts of the Gabgaba Terrane. Recently, Saeed et al. [13] studied the granitoids in the northern segment of the Gabgaba Terrane. They differentiated between two granitic groups: the older I-type (~663 Ma, U-Pb age) and the younger A-type (623.5 Ma; U-Pb zircon) granites. They argue that these granitoids were produced by partial melting of subduction-modified materials. In the southern tip of the Gabgaba Terrane (Haweit area), older ages were recorded from andesite (752 ± 11 Ma; U-Pb zircon) and basaltic andesite rocks (773 ± 17 Ma; U-Pb zircon) [25].

The Haweit area belongs to the Gabgaba Terrane and located in the southern part of the HSZ (Figure 1B). The area is covered by a variety of crystalline rocks represented mainly by granites. There are no detailed studies about the nature of granitic rocks in the Haweit area, and the only published works by Adam et al. [24,25] deal with the gold mineralization and mafic intrusions in the area. Therefore, in this contribution, we provide new bulk rock geochemistry and geochronological (zircon U-Pb and Lu-Hf isotopes) data from the Haweit I-type granites. The aim is to constrain the crystallization age and discuss the petrogenesis, magma source, and the tectonic setting of these granitic rocks. This research enhances our knowledge about crustal development in NE Sudan (in particular) and the ANS (in general) during the Neoproterozoic.

2. Geological Background and Petrography

The ANS comprises variable magmatic rock units, which are widely distributed in many countries located in the region surrounding the Red Sea, including Sudan, Yemen, Somalia, Saudi Arabia, Egypt, and Jordan (Figure 1A). The ANS is primarily made up of Neoproterozoic (900–550 Ma) juvenile arc terranes [27]. The ANS was generated by the welding of oceanic island arc, back-arc basins, and ophiolites [28–31]. This composite arc continent is formed between E and W Gondwana's large continental blocks. The ANS cratonization and stabilization were completed during the late Ediacaran–early Cambrian. The rock sequences that make up the ANS are well recognized in terms of lithology: ophiolites, quartzo-feldspathic varieties, island arcs, and supracrustal intrusive suites. Subsequently, subduction and late- to post-collisional magmatism generated several gabbroic and granitoid intrusions and associated volcanics. The calc-alkaline granitoids were developed before the ANS experienced substantial crustal extension. The ANS was affected by several extensional tectonic structures as represented by basins bordered by faults and filled with molasses, core complexes, and major thrust fault. The northern part of the ANS was subject to extensional tectonics, shearing, and thrusting, which developed predominantly northwest structural trends (Najd fault system) which affected both the Egyptian Eastern Desert and the Arabian Shield. Related to this is east–west compression leading to the development of the HSZ [16] (Figure 1B).

The HSZ has a N–S trend and is clearly distinguished from the Sol Hamed (NE–SW trending) and Allaqi–Heiani (NE–SW trending) sutures [32]. The HSZ is a high-strain zone with only small wrench-faulting components. Deformation is characterized by strong shearing, which results in E–W shortening and a significant N–S extensional portion. After suturing of the Gabgaba Terrane with the other terranes in the north, the E–W shortening that created the HSZ took place. The HSZ has been interpreted as a strike-slip deformation or a collision-related crustal shortening zone [33]. The north segment of HSZ was still active until around 550 Ma [33]. Although collisional suturing and terrane assembly in the ANS are 50–150 Ma older than activity in the HSZ, it is roughly contemporaneous with that of the 630–580 Ma Najd fault system in Egypt and Arabia. Furthermore, the Najd tectonic cycle is likely connected to the metamorphism and deformation along the HSZ, which postdate terrane accretion. The HSZ encompasses gneisses that overlain structurally by

ophiolitic sequences and intruded by variable granitic masses. The oldest exposed rocks are most likely a succession of multicolored gneisses, followed by the intrusion of basic and intermediate rocks. A series of syn- to late-orogenic granitic plutons and dyke swarms fold and intrude on each of these oldest rock units [16].

The Haweit area lies within the Red Sea Hills of NE Sudan on the eastern margin of the Gabgaba Terrane (Figure 2A). The Keraf Suture Zone borders the terrane to the west, while the HSZ borders it to the east (Figure 1A). The Gabgaba Terrane is poorly known but seems to be mainly composed of Neoproterozoic low-grade metamorphic rocks (dominantly greenschist facies), an island arc assemblage (metavolcanics and marble bands), and intruded by granitic plutons [25,34]. Crystalline magmatic rocks underlie the greater part of the study area and crop out widely in the middle, eastern, and northern parts (Figure 2A).

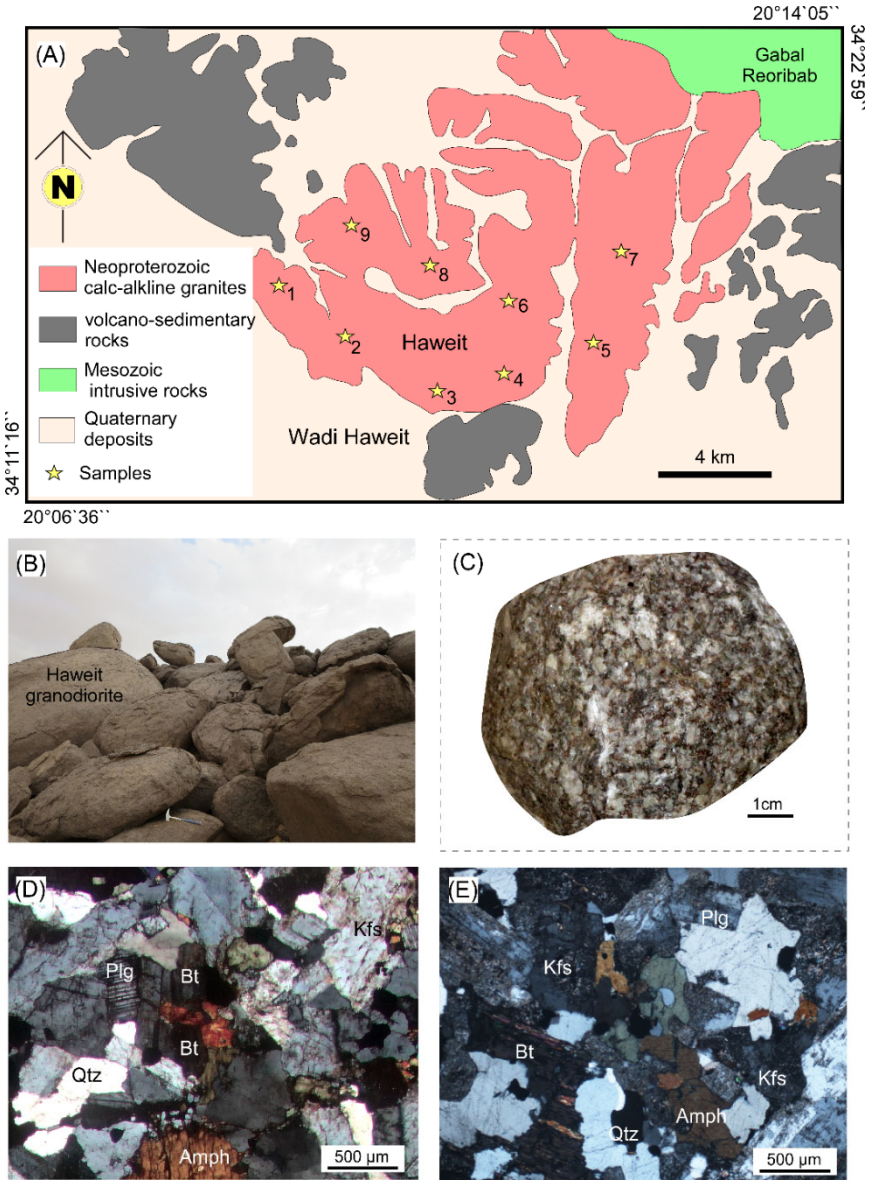

Figure 2. (**A**) Geological map of the Haweit area showing lithological units and samples location. Dated zircon crystals were separated from the fresh granitic sample (HG6); (**B**) field photograph showing the boulder appearance of the Haweit low hills granodiorites; (**C**) macroscopic image of granodiorite hand specimen; (**D**,**E**) photomicrograph (XPL) showing the main minerals components and the hypidiomorphic texture of the granodiorite, Pl—plagioclase, Qtz—quartz, Kfs—k-feldspar, Amph—amphibole, Bt—biotite.

The basement complex consists of Neoproterozoic low-grade metamorphosed volcano-sedimentary assemblages and granodioritic to gabbroic plutonic rocks. Basement rocks are overlain by undeformed Mesozoic to Cenozoic volcanics and sedimentary strata and a younger superficial cover. Basement rocks comprise greenschist-grade, metasedimentary, and metavolcanic rocks, deformed to schist and gneiss, and intruded by multiple generations of granitoids [35]. The Haweit granodiorites occurred as low hilly outcrops that intruded into the andesite and basaltic andesites and are characterized by their blocky and bouldery appearance (Figure 2B).

Petrographically, granites are light gray and medium- to coarse-grained with a hypidiomorphic texture (Figure 2C–E). They are made up of a proportion of plagioclase (48–39 vol.%), K-feldspar (17–10 vol.%), quartz (25–21 vol.%), biotite (12–8 vol.%), and amphibole (6–3 vol.%) as the major mineral phases. The mafic minerals fill the intersections between plagioclase crystals (Figure 2D–E). Accessory minerals are epidote, Fe-Ti oxides, apatite, titanite, and zircon. Chlorite and sericite are the main alterations and post-solidus products, replacing biotite and plagioclase, respectively. Plagioclase is a widespread mineral that occurs essentially as euhedral to subhedral grains and shows polysynthetic twins. Amphiboles are subhedral to euhedral and commonly contain apatite, quartz, and Fe-Ti oxides inclusions. Biotite commonly exists as euhedral to subhedral flakes interstitial to quartz and feldspars and occasionally forms aggregates with amphibole.

3. Analytical Methods

Before conducting U-Pb dating and Hf isotope measurements, the internal structure of zircon crystals was studied using an electron microprobe (CAMECA SX51; Langfang Regional Geological Survey in Hebei Province, China). The zircon U-Pb and Lu-Hf isotopes were, respectively, measured using an Agilent 7700a ICP-MS (inductively coupled plasma mass spectrometer) and a Neptune Plus MC-ICP-MS at the State Key Laboratory of Geological Processes and Mineral Resources of the China University of Geosciences (Wuhan). The whole rock geochemical data were performed at ALS Chemex Company Ltd. in Guangzhou (China) using a PAN analytical Axios X-ray fluorescence spectrometer (XRF). A complete description of the methodology, operating conditions, procedures, and standards used in this work is provided in the online Supplementary Document S1.

4. Results

4.1. Zircon Morphology and U-Pb Dating

The cathodoluminescence (CL) images of some typical zircon grains are displayed in Figure 3A and Table 1 lists the LA-ICP-MS analytical data of the separated zircons. Zircons are euhedral and prismatic, and their lengths range from 80 to 180 μm. Their colors range from white to translucent. The zircons have an internal oscillatory zonation, indicating magmatic origin [36]. Twenty-two spot analyses were performed (Table 1). Variable Th (270–3002 ppm) and U (554–8382 ppm) values were found, with Th/U ratios ranging from 0.25 to 1.24. Due to Pb loss and the common Pb effect, some analyses have a high degree of discordance (either visible or invisible). For age estimation, these U-Pb analyses were ignored. Thirteen U-Pb date analyses are frequently concordant (>95% concordance) and yield a Concordia age of 718.5 ± 2.2 Ma (MSWD = 0.97; n = 13) (Figure 3B), which is regarded as the crystallization age of the investigated granodiorites.

Table 1. Zircon U-Pb isotopic dating data from the Haweit granodiorites, NE Sudan.

Grain	Th (ppm)	U (ppm)	Th/U	Isotopic Ratios						Apparent Ages (Ma)				
				$^{207}Pb/^{206}Pb$	1σ	$^{207}Pb/^{235}U$	1σ	$^{206}Pb/^{238}U$	1σ	$^{207}Pb/^{235}U$	1σ	$^{206}Pb/^{238}U$	1σ	Conc%
HG-01	684	1681	0.41	0.071951	0.002303	1.122183	0.048025	0.110981	0.001669	764	23	678	10	88%
HG-02 *	327	1043	0.31	0.062032	0.001613	0.992674	0.026553	0.115796	0.001730	700	14	706	10	99%
HG-03	778	1239	0.63	0.069836	0.001975	0.998715	0.032159	0.102915	0.001466	703	16	631	9	89%
HG-04 *	567	871	0.65	0.063751	0.002428	1.087243	0.051132	0.118599	0.001258	747	74	722	14	96%
HG-05	603	896	0.67	0.067973	0.002475	1.090820	0.048106	0.114938	0.001920	749	23	701	11	93%
HG-06 *	1699	5268	0.32	0.064359	0.001544	1.060474	0.029404	0.118855	0.001408	734	14	724	8	98%
HG-07 *	2125	5521	0.38	0.063863	0.001958	1.068074	0.038638	0.120883	0.001942	738	19	736	11	99%
HG-08	2997	2418	1.24	0.066856	0.001881	0.953077	0.027434	0.102372	0.001306	680	14	628	8	92%
HG-09	3002	8382	0.36	0.077196	0.002000	1.160365	0.033885	0.107787	0.002290	782	16	660	13	83%
HG-10 *	472	1660	0.28	0.061970	0.001882	0.997502	0.032758	0.116906	0.001849	703	17	713	11	98%
HG-11 *	799	2853	0.28	0.063721	0.001204	1.024503	0.020251	0.116564	0.001916	716	10	709	11	99%
HG-12 *	1883	4829	0.39	0.065509	0.001628	1.045052	0.031053	0.116627	0.001629	728	16	712	10	98%
HG-13	1435	2889	0.50	0.089446	0.002187	1.509540	0.043476	0.120787	0.001608	934	18	735	9	76%
HG-14	859	1562	0.55	0.063245	0.005642	0.871739	0.074914	0.099064	0.003667	637	41	609	22	95%
HG-15 *	1754	3189	0.55	0.065369	0.002518	1.045109	0.040574	0.116904	0.002606	726	20	711	14	98%
HG-16 *	716	981	0.73	0.063628	0.001751	1.032021	0.023615	0.116202	0.001469	719	13	709	9	99%
HG-17 *	446	554	0.81	0.065461	0.014180	1.052993	0.023474	0.116476	0.002704	731	12	708	13	98%
HG-18	620	2443	0.25	0.067220	0.001836	1.073239	0.032842	0.114563	0.001356	740	16	699	8	94%
HG-19 *	270	1009	0.27	0.065454	0.001434	1.052563	0.022822	0.115383	0.002503	732	13	706	14	99%
HG-20	1100	2086	0.53	0.072646	0.010497	0.880401	0.056281	0.101147	0.007999	641	30	621	47	96%
HG-21 *	592	1057	0.56	0.065925	0.000906	1.046208	0.015941	0.115628	0.001615	727	8	706	10	97%
HG-22 *	391	954	0.41	0.066691	0.000891	1.067519	0.021624	0.116517	0.001835	735	12	711	12	98%

* U-Pb date analyses used in age calculation.

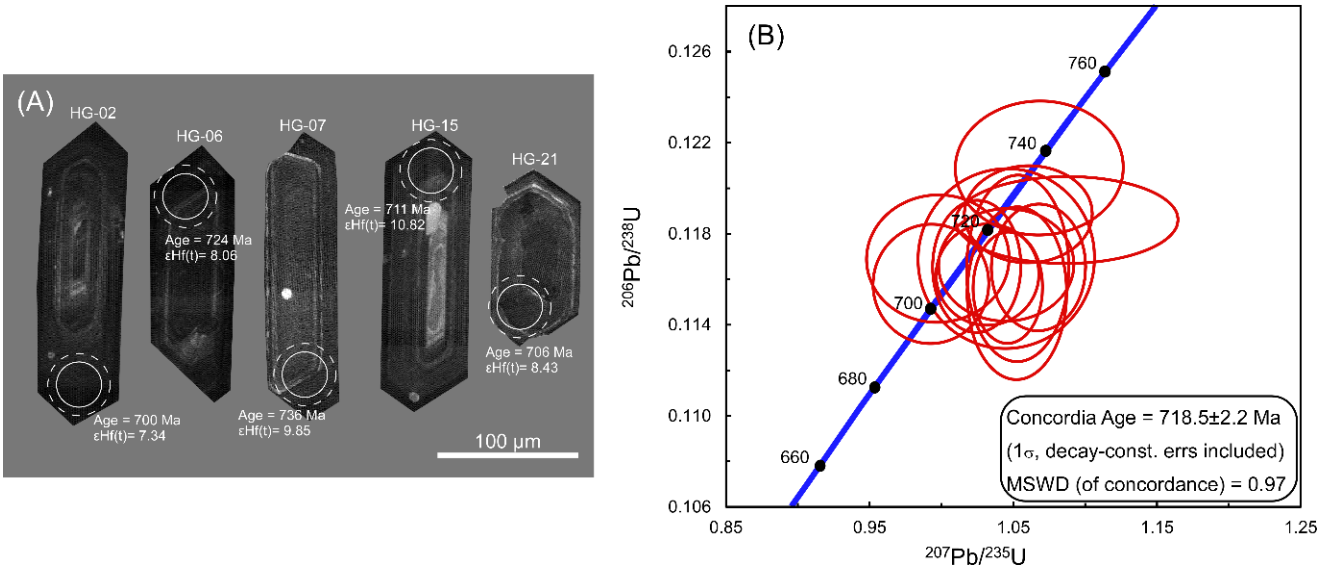

Figure 3. (**A**) Cathodoluminescence (CL) images of representative zircon grains of the Haweit granodiorites, showing inner structures and the laser analytic spots, $^{206}Pb/^{238}U$ ages, and εHf(t) values. Solid white circles show the locations of U-Pb age analyses, and dotted circles show the locations of Lu-Hf isotope analyses; (**B**) zircon U-Pb Concordia diagram for the analyzed zircons.

4.2. Whole-Rock Geochemical Compositions

The concentrations of the major oxides (in wt.%), trace, and REE elements (in ppm) of the representative samples from the Haweit area are listed in Table 2. Petrographic examination reveals that the Haweit granodiorites are fresh, with a limited evident secondary modification. These findings are in line with the low loss of the ignition (LOI) content (usually less than 1 wt.%, Table 2) and suggest that the samples sustained no major changes that would influence the distribution and abundance of petrogenetic-indicating REEs and high-field-strength elements (HFSE). The samples are plotted into the field of granodiorite in the SiO_2 vs. $Na_2O + K_2O$ diagram (Figure 4A). The granodiorites are characterized by their intermediate SiO_2 (64.14–69.18 wt.%), medium K_2O (1.41–2.48 wt.%), and high Na_2O/K_2O ratio (2.01–3.84). The granodiorites have a calc-alkaline composition (Figure 4B,C) with a metaluminous signature (A/CNK = 0.84–0.94) (Figure 4D), similar to the other granodiorites over the Nubian Shield. Compared to typical fractionated granitoids in the ANS, the samples display high $Fe_2O_3{}^t$ (4.33–6.17 wt.%), Al_2O_3 (14.09–15.41 wt.%), Na_2O (4.76–5.41 wt.%), Y (14–46 ppm), Rb (48–93 ppm), and Ba (418–602 ppm), with a moderate content of CaO (2.57–3.94 wt. %) and Sr (191–318 ppm). They have a notable depletion in K_2O, Cr, V, Ti, Nb, Ta, Hf, Ta, and heavy REEs (HREEs).

The Harker variation diagrams (Figure 5) display a remarkable decrease in Fe_2O_3, CaO, TiO_2, and Zr contents, similar to other granodiorites from the Nubian Shield. In the primitive mantle normalized spider diagram (Figure 6A), all samples are enriched in LILEs (Rb, Th, and U) and depleted in Nb, Ta, Sr, P, and Ti. Moreover, the samples show enrichment of LREE with $(La/Yb)_N$ = 3.0–5.9 and a flat HREE pattern (Figure 6B) with low $(Gd/Yb)_N$ = 0.86–1.75 (Table 2). Their chondrite normalized REE patterns are similar to arc granitoids with low negative Eu anomalies (Eu/Eu* = 0.42–0.80). Overall, the samples exhibit arc granitoid characteristics such as negative Ti, Ta, and Nb anomalies, as well as enrichment in LILE (Rb, Ba, U, and Th) and LREE (e.g., Ce and La) (Figure 6A,B). In general, the geochemical characteristics of the Haweit granodiorites are comparable to those of the Eastern Desert I-type granitoids, and arc-related granitoids worldwide (Figures 4–6).

Table 2. Analytical data of whole-rock major and trace elements and related parameters of the Haweit granodiorites, NE Sudan.

Sample	HG1	HG2	HG3	HG4	HG5	HG6	HG7	HG8	HG9
SiO_2	64.14	65.19	66.12	67.05	66.57	67.76	68.77	69.18	69.07
TiO_2	1.02	0.95	0.84	0.81	0.79	0.78	0.76	0.62	0.59
Al_2O_3	15.41	15.37	14.99	14.35	14.71	14.98	14.69	14.38	14.09
MgO	1.18	0.72	1.06	1.31	1.16	0.78	0.71	0.68	0.57
Fe_2O_3	6.17	5.88	5.29	4.94	4.82	4.61	4.33	4.36	4.47
CaO	3.94	3.47	3.72	3.11	3.22	3.28	2.97	2.72	2.57
Na_2O	5.41	5.31	4.96	4.76	4.86	4.98	5.03	4.94	4.99
K_2O	1.41	1.82	1.98	2.24	2.39	1.68	1.93	2.15	2.48
MnO	0.11	0.08	0.08	0.09	0.08	0.07	0.07	0.08	0.07
P_2O_5	0.33	0.28	0.23	0.17	0.21	0.18	0.17	0.19	0.18
LOI	0.76	0.94	0.84	0.89	0.83	0.81	0.89	0.88	0.97
Sum	99.88	100.01	100.1	99.72	99.64	99.91	100.3	100.2	100.1
V	29.3	28.4	21.6	20	21.3	25.6	23.0	24.9	20.2
Cr	6.7	5.6	4.5	4.9	4.6	4.4	4.8	4.3	4.1
Ga	19.5	19.5	19.2	2.0	19.6	18.2	19.0	18.4	18.7
Rb	48	63	65	68	69	75	71	73	93
Sr	314	318	269	221	209	216	228	194	191
Y	14	17	22	25	29	35	32	41	46
Zr	217	247	201	172	217	223	210	216	205
Nb	7.78	8.35	6.72	6.04	6.77	8.69	8.13	8.53	7.9
Cs	0.15	0.22	0.31	0.37	0.34	0.42	0.52	0.94	0.81
Ba	457	528	481	437	473	602	599	418	455
La	21	30	24	22	26	28	28	27	34
Ce	56	70	55	50	55	69	65	61	75
Pr	8.37	9.32	7.75	6.64	7.11	9.78	8.78	7.37	8.81
Nd	37	38	31	27	28	40	36	30	33
Sm	9.35	8.39	7.27	6.23	6.77	8.83	7.94	6.95	7.19
Eu	2.02	2.08	1.58	1.34	1.44	1.91	1.82	0.93	0.98
Gd	8.73	7.52	6.57	5.74	6.01	7.45	7.03	6.53	5.86
Tb	1.42	1.09	1.06	0.91	0.98	1.12	1.04	1.18	1.31
Dy	8.03	6.21	6.11	5.22	5.81	6.55	5.97	7.33	6.16
Ho	1.71	1.27	1.26	1.08	1.19	1.28	1.22	1.62	1.39
Er	4.61	3.56	3.49	3.04	3.46	3.69	3.36	5.06	4.12
Tm	0.71	0.52	0.57	0.47	0.53	0.55	0.49	0.84	0.74
Yb	4.81	3.47	3.56	3.32	3.53	3.66	3.29	6.11	5.01
Lu	0.72	0.52	0.57	0.51	0.59	0.54	0.55	1.01	0.84
Hf	11.3	8.6	9.2	9.8	10.4	9.5	9.6	9.2	8.3
Ta	0.5	0.5	0.6	0.5	0.6	0.6	0.5	0.8	0.7
Th	4.6	6.4	4.8	4.9	5.8	6.5	5.7	7.4	6.9
U	2.1	3.2	2.5	2.4	2.8	3.2	3	5.8	5.2
A/CNK	0.88	0.90	0.86	0.90	0.84	0.94	0.93	0.93	0.91
K_2O/Na_2O	0.26	0.34	0.40	0.47	0.49	0.34	0.38	0.44	0.50
Eu/Eu*	0.67	0.8	0.7	0.68	0.67	0.72	0.74	0.42	0.44
∑REE	165	182	149	134	144	182	170	161	183
$(La/Yb)_N$	3	5.91	4.48	4.44	4.54	5.25	5.7	3.02	4.66
$(Gd/Yb)_N$	1.46	1.75	1.49	1.4	1.38	1.65	1.73	0.86	0.95
$(Y/Nb)_N$	0.88	0.63	0.73	0.76	0.76	0.62	0.61	0.87	0.75

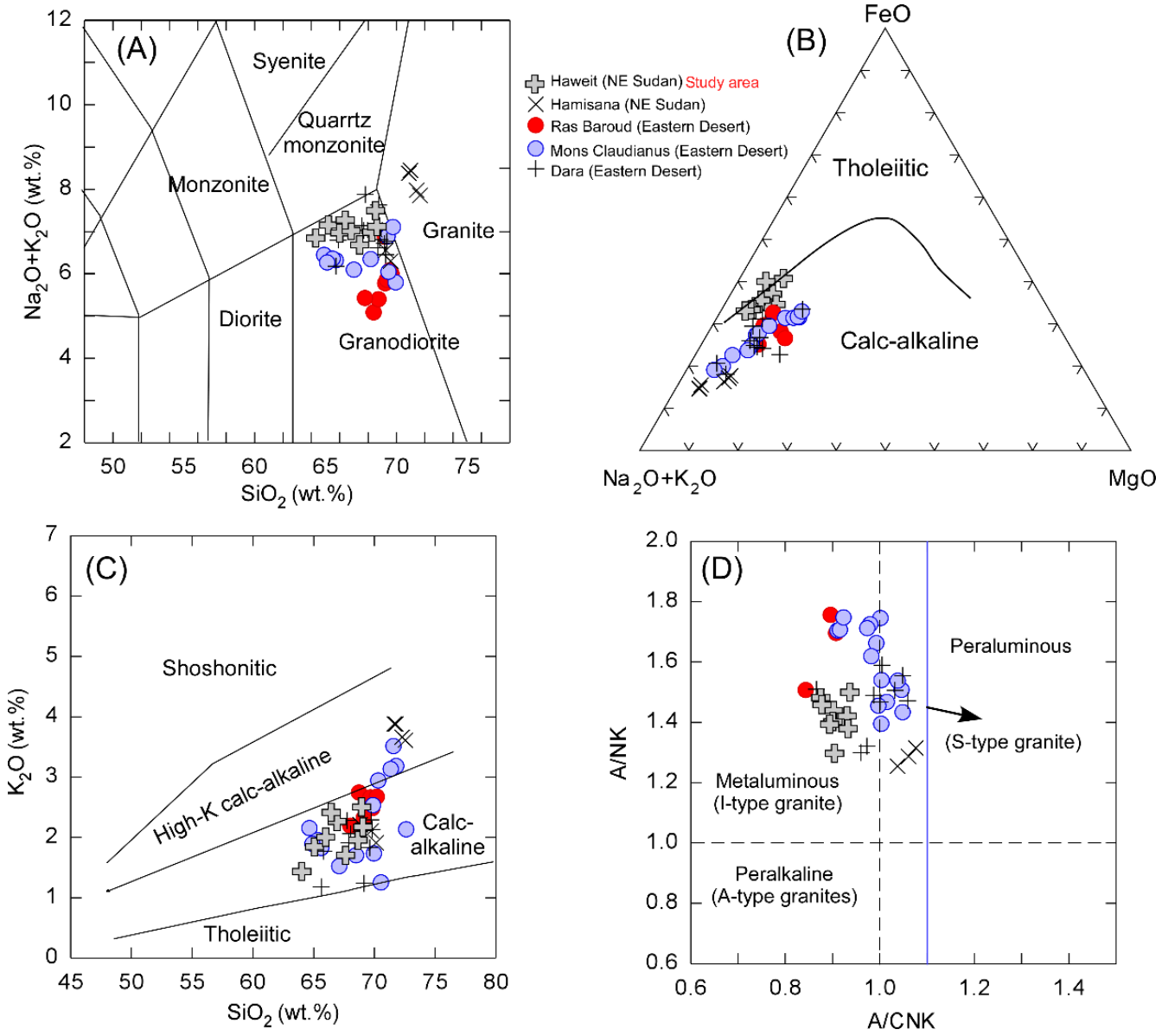

Figure 4. Whole-rock composition of the Haweit granodiorite. (**A**) TAS diagram [37], showing the classification of the studied granodiorites; (**B**) discrimination diagrams $Na_2O + K_2O$-FeO-MgO ternary diagram for tholeiitic and calc-alkaline magma series [38]; (**C**) K_2O versus SiO_2 diagram [39]; and (**D**) A/NK (molar $Al_2O_3/Na_2O + K_2O$) vs. A/CNK (molar $Al_2O_3/CaO + Na_2O + K_2O$) [40], showing that almost all samples have a metaluminous signature. The data of other granodiorite samples from various localities in the Nubian Shield, including Hamisana [13], Ras Baroud [41], Mons Claudianus [42], and Dara [43], are used for comparison.

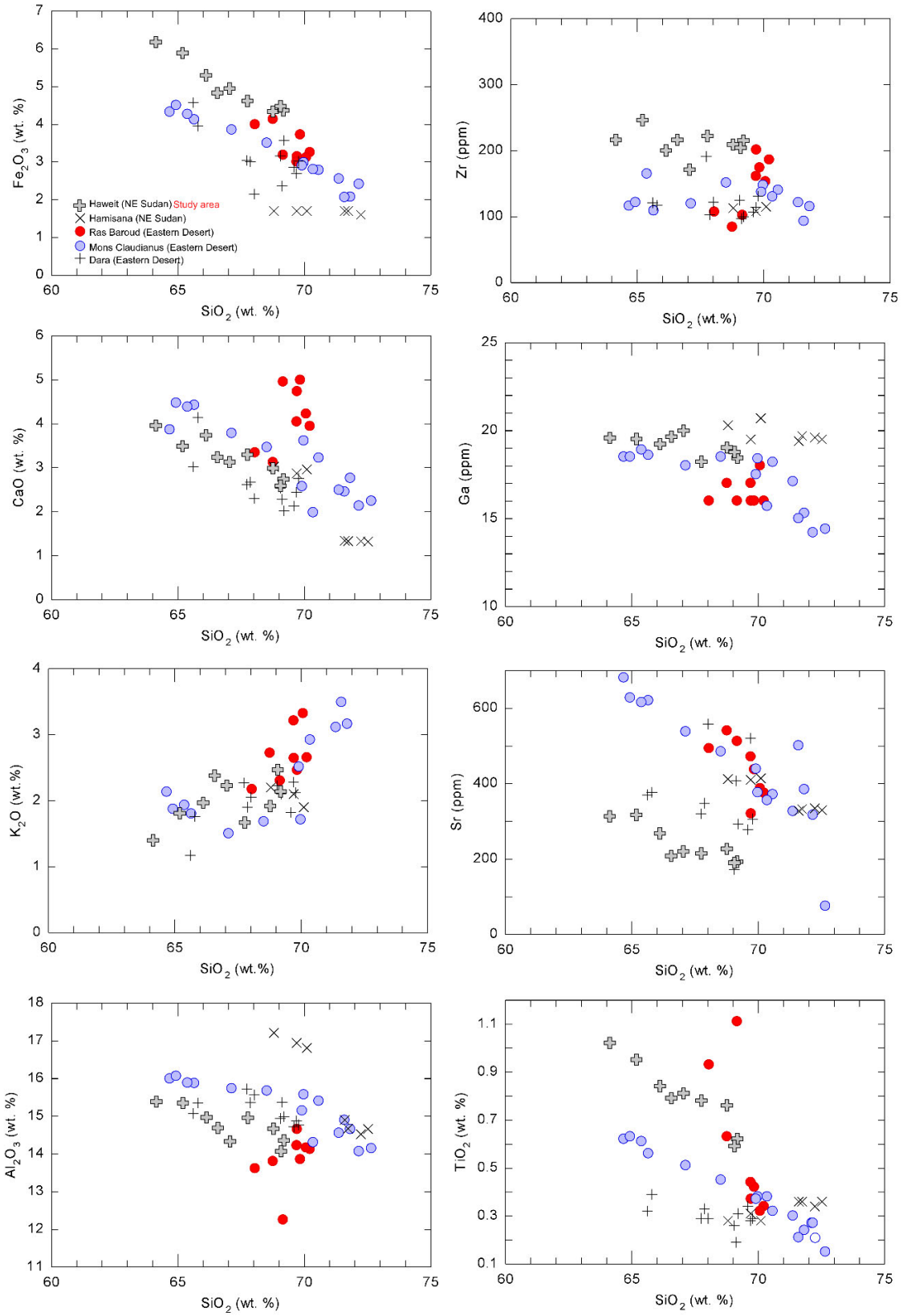

Figure 5. Harker variations of selected major (Fe_2O_3, CaO, Al_2O_3, K_2O, and TiO_2) and trace (Zr, Ga, and Sr) elements vs. SiO_2. The data of other granodiorite samples from various localities in the Nubian Shield, including Hamisana [13], Ras Baroud [41], Mons Claudianus [42], and Dara [43], are used for comparison.

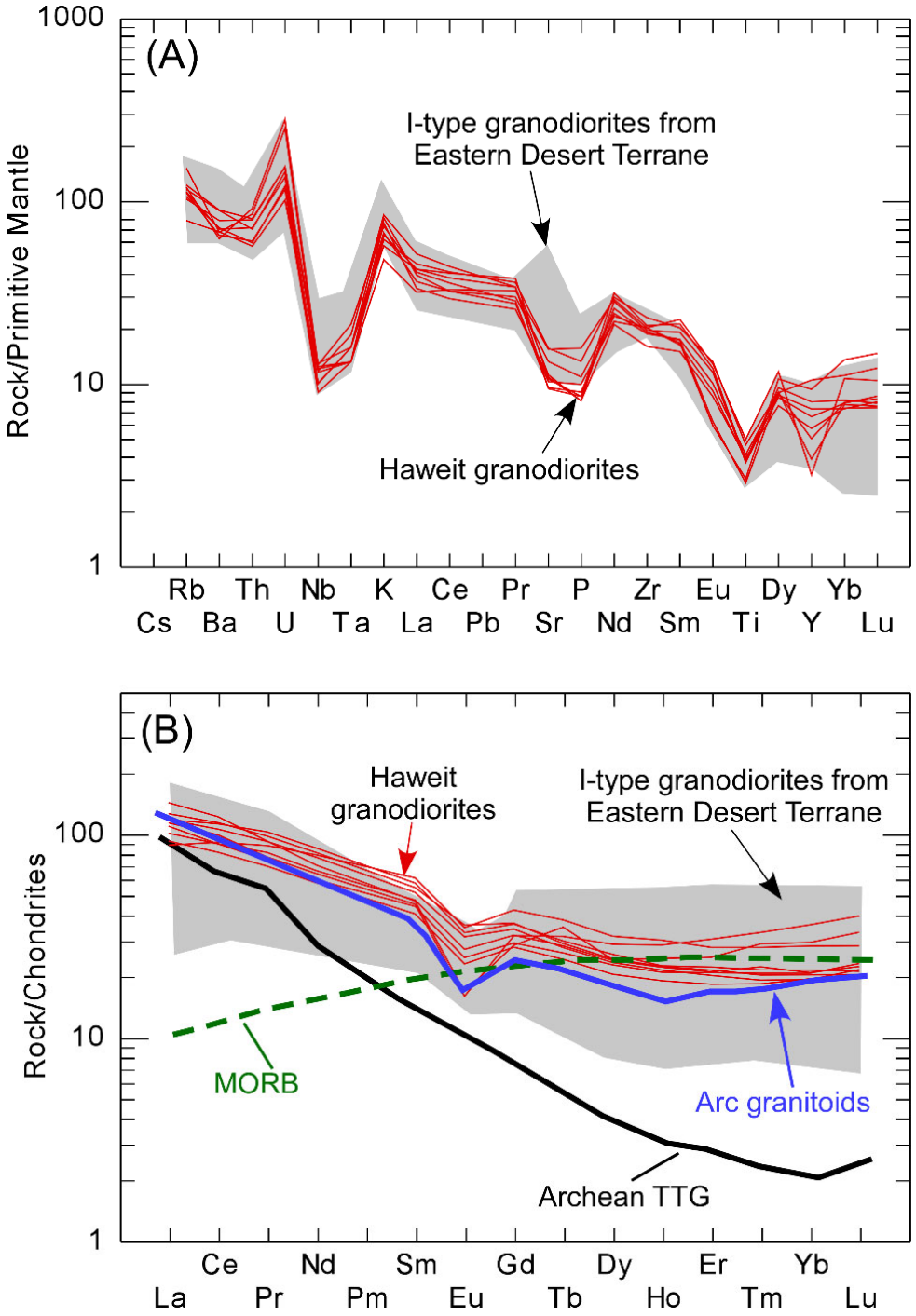

Figure 6. (**A**) Multi-elements spider diagrams normalized to the primitive mantle; (**B**) REEs patterns normalized to chondrite for the Haweit granodiorite. The normalization values of both primitive mantle and chondrite are from Sun and McDonough [44]. The data of mid-oceanic ridge basalt (MORB; [44]), arc granitoids [3], and Archaen tonalite–trondhjemite–granodiorite (TTG; [45]) are presented. The field of I-type granodiorites from the Eastern Desert is adopted from El-Bialy and Omar [41] and Abdel-Rahman [42].

4.3. Zircon Lu-Hf Isotopes

In silicate melts, the Lu-Hf and Sm-Nd isotopes exhibited nearly identical behavior. Moreover, Lu and Hf are immobile trace elements that are not significantly redistributed by thermal events, permitting the isotopic ratios of their source areas to be preserved [46]. Hf isotopes in zircons, on the other hand, are frequently used to determine magma origins [47].

In granitoids, zircon is the most common host of Hf (~1 wt. %) and it contains trace amounts of Lu (in ppm) [36].

Because zircons have extremely low $^{176}Lu/^{177}Hf$ isotope ratios, their current (present-day) isotopic proportions strongly match those of the magmas from which the zircons originated [48]. The zircon Hf isotopic ratios in granitoids provide a clear indication of the source, with the continental crust having a high $^{176}Lu/^{177}Hf$ ratio and depleted mantle having a low $^{176}Lu/^{177}Hf$ ratio [49].

The results of twelve single zircons examined for Lu-Hf isotopes at identical U-Pb dated sites are summarized in Table 3 and shown in Figure 7. The zircons (ca. 719 Ma) display $^{176}Hf/^{177}Hf$ values ranging from 0.282553 to 0.282682, $^{176}Lu/^{177}Hf$ values from 0.000296 to 0.003960, and $^{176}Yb/^{177}Hf$ ratios ranging from 0.011109 to 0.121202. Their initial εHf(t) values fluctuate between +7.3 and +11.2 (Figure 7), with a corresponding single-stage Hf model age of 728–885 Ma and crustal Hf model ages (Hf-t_{DM}^{C}) of 734–985 Ma (Table 3).

Table 3. Single zircon Lu–Hf isotopic data for Haweit granodiorites from NE Sudan.

Grain No#	t (Ma)	$^{176}Yb/^{177}Hf$	1σ	$^{176}Lu/^{177}Hf$	1σ	$^{176}Hf/^{177}Hf$	1σ	εHf(0)	εHf(t)	t_{DM1}	t^{c}_{DM}	$f_{Lu/Hf}$
HG-02	719	0.055252	0.001842	0.001640	0.000046	0.282553	0.000034	−7.75	7.34	885	985	−0.95
HG-04	719	0.078755	0.001712	0.002171	0.000034	0.282561	0.000046	−7.45	7.39	885	981	−0.93
HG-06	719	0.044282	0.001068	0.001303	0.000025	0.282568	0.000024	−7.20	8.06	855	939	−0.96
HG-07	719	0.011551	0.000050	0.000308	0.000000	0.282606	0.000034	−5.88	9.85	781	822	−0.99
HG-10	719	0.086647	0.002029	0.002568	0.000055	0.282655	0.000032	−4.15	10.51	757	779	−0.92
HG-11	719	0.058733	0.001180	0.002066	0.000045	0.282617	0.000041	−5.50	9.40	802	851	−0.94
HG-12	719	0.032830	0.000163	0.000989	0.000002	0.282653	0.000027	−4.21	11.21	728	734	−0.97
HG-15	719	0.121202	0.001186	0.003960	0.000027	0.282682	0.000052	−3.17	10.82	746	759	−0.88
HG-16	719	0.053642	0.000269	0.001343	0.000001	0.282641	0.000055	−4.63	10.61	752	772	−0.96
HG-17	719	0.011109	0.000046	0.000296	0.000001	0.282565	0.000029	−7.31	8.43	836	915	−0.99
HG-19	719	0.066214	0.003906	0.002018	0.000102	0.282594	0.000026	−6.30	8.62	834	902	−0.94
HG-21	719	0.013041	0.000032	0.000348	0.000001	0.282566	0.000027	−7.29	8.43	837	915	−0.99

Initial Hf isotope ratios were calculated with reference to the chondritic ratio at the time of crystallization assumed for each sample, a decay constant for ^{176}Lu of 1.867×10^{-11}, and the chondritic ratios of $^{176}Hf/^{177}Hf$ (0.282772) and $^{176}Lu/^{177}Hf$ (0.0332) were used. Single-stage Hf model ages (t_{DM}) were calculated using the measured ratios, referring to a model depleted mantle with present-day $^{176}Hf/^{177}Hf$ of 0.28325 and $^{176}Lu/^{177}Hf$ of 0.0384. Two-stage Hf model ages (t_{DM}^{c}) are calculated, assuming a mean $^{176}Lu/^{177}Hf$ value of 0.015 for average continental crust.

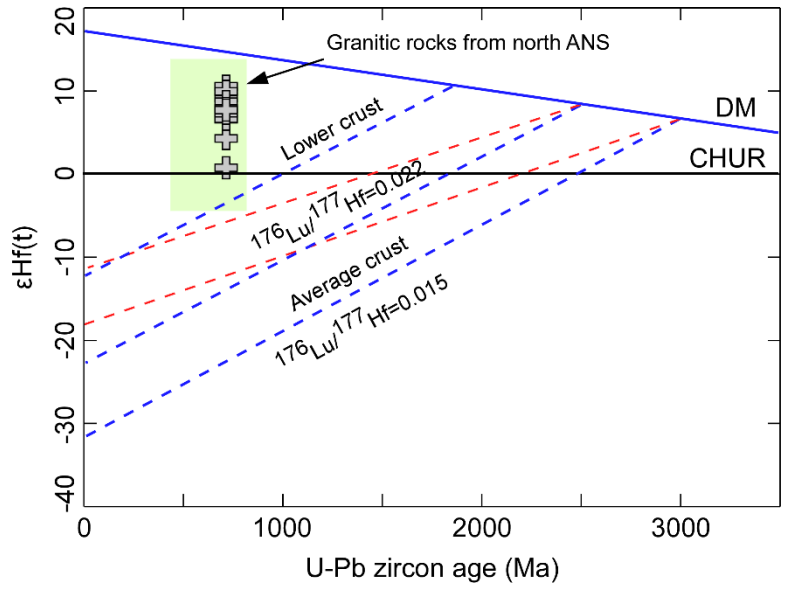

Figure 7. Epsilon Hf(t) versus age diagram showing zircon data for the Haweit granodiorite. The depleted mantle (DM) growth curve (solid line) was extrapolated from average modern-day values of $^{176}Hf/^{177}Hf = 0.28325$ and $^{176}Lu/^{177}Hf = 0.0334$. CHUR is the chondritic uniform reservoir. The field of granitoids from north ANS is adopted from Ali et al. [50].

5. Discussion

5.1. Timing of Emplacement and Hf-Lu Isotopic Signatures

This is the first approach to date the granodiorites in the Haweit area using U-Pb zircon isotopes. Most zircon crystals show an internal oscillatory zoning (Figure 3A) with high Th/U ratios (Table 1), indicating an igneous origin. The dated zircons present a Concordia age of 718.5 ± 2.2 Ma (Figure 3B); this confirms that the Haweit granodiorites were emplaced and crystallized during Cryogenian time. It is worth noting that the ages of the Haweit granodiorites are more or less in the range of the previously reported U-Pb zircon ages from other Neoproterozoic granitic intrusions distributed over the ANS, such as the Dara granodiorites (720.2 ± 7.1 Ma; [43]) and Wadi Beitan granodiorites (725 ± 9 Ma; [50]).

The zircon Lu-Hf isotopic results of the present study rule out the input of a pre-Neoproterozoic source in the genesis of the investigated granodiorites (Figure 8). Whereas zircon U-Pb dating is vital for establishing the age of the protolith, zircon Lu-Hf isotope ratios are commonly used to identify the characteristics of the protolith [51]. The substantial discrepancies in the Hf-isotope concentration of zircon grains of an identical age can be attributed to either the melting of heterogeneous crust or a mix between crust- and mantle-derived magmas [52]. The analyzed zircons yielded a young age (t_{DM}^{C} = 734–985 Ma), which is relatively close to the time of granodiorite formation. The calculated Hf model age (Table 3) indicates a juvenile composition of the granodiorites and proves that their protolith is not affected by old crustal rocks (Figure 8). The zircon Hf isotopic values from the Haweit granodiorites are comparable to those found in granitoids from many ANS locations [50]. The zircon Hf isotopes suggest that zircons were probably crystallized in a homogenous granitic magma where zircons have, within error, more or less the same initial Lu-Hf isotopic ratio [50]. The U-Pb zircon age of the Haweit granodiorites (718.5 Ma; Figure 3B) and the Lu-Hf isotopic results (Figures 7 and 8) suggest that the granitoids in NE Sudan were probably formed during magmatic arc evolution.

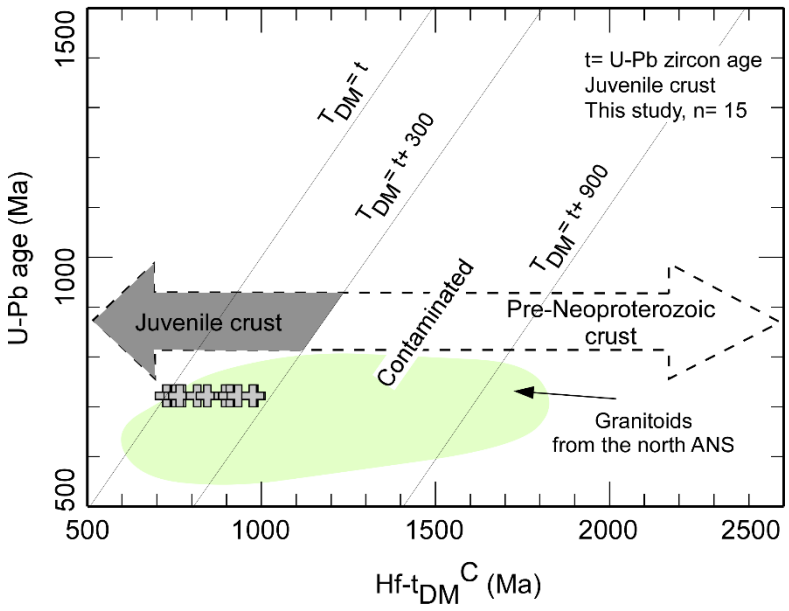

Figure 8. Plots of U–Pb zircon ages versus Hf crustal model ages (Hf-t_{DM}^{C}) (modified after Hargrove et al. [53]) for zircons from the Haweit granodiorite. Crustal model ages (t_{DM}^{C}; Table 3) were calculated assuming that the parental magma of the zircons was produced from an average continental crust ($^{176}Lu/^{177}Hf$ = 0.010) [54]. Data yielding Hf-t_{DM}^{C} = t (U-Pb zircon age) or Hf-t_{DM}^{C} < t are considered to represent a juvenile source, whereas those with t + 300 < Hf-t_{DM}^{C} < t + 900 or with Hf-t_{DM}^{C} > t + 900 are considered to represent juvenile crust contaminated by pre-Neoproterozoic crustal components.

5.2. Genetic Type of Haweit Granodiorites

Granitic rocks have been generally divided into I-, S-, and A-types according to their mineralogical composition, nature of the protolith, and geochemical characteristics [55]. The most significant indicator for distinguishing granite types is the prevalence of distinctive minerals. High-temperature anhydrous minerals (e.g., pyroxene and interstitial biotite) distinguish the A-type granites. S-type granites are known to be rich in inherited zircon and Al-rich minerals (e.g., muscovite and cordierite). I-type granites, on the other hand, were found to be generated from meta-igneous rocks and to include amphibole. Petrographically, the Haweit granodiorites contain both biotite and amphibole as the main mafic constituents (Figure 2D,E), implying an I-type affinity. In the binary diagram of K_2O vs. Na_2O (Figure 9A), all samples along with other typical I-type granodiorites from the Nubian shield plot in the I-type granites field [6].

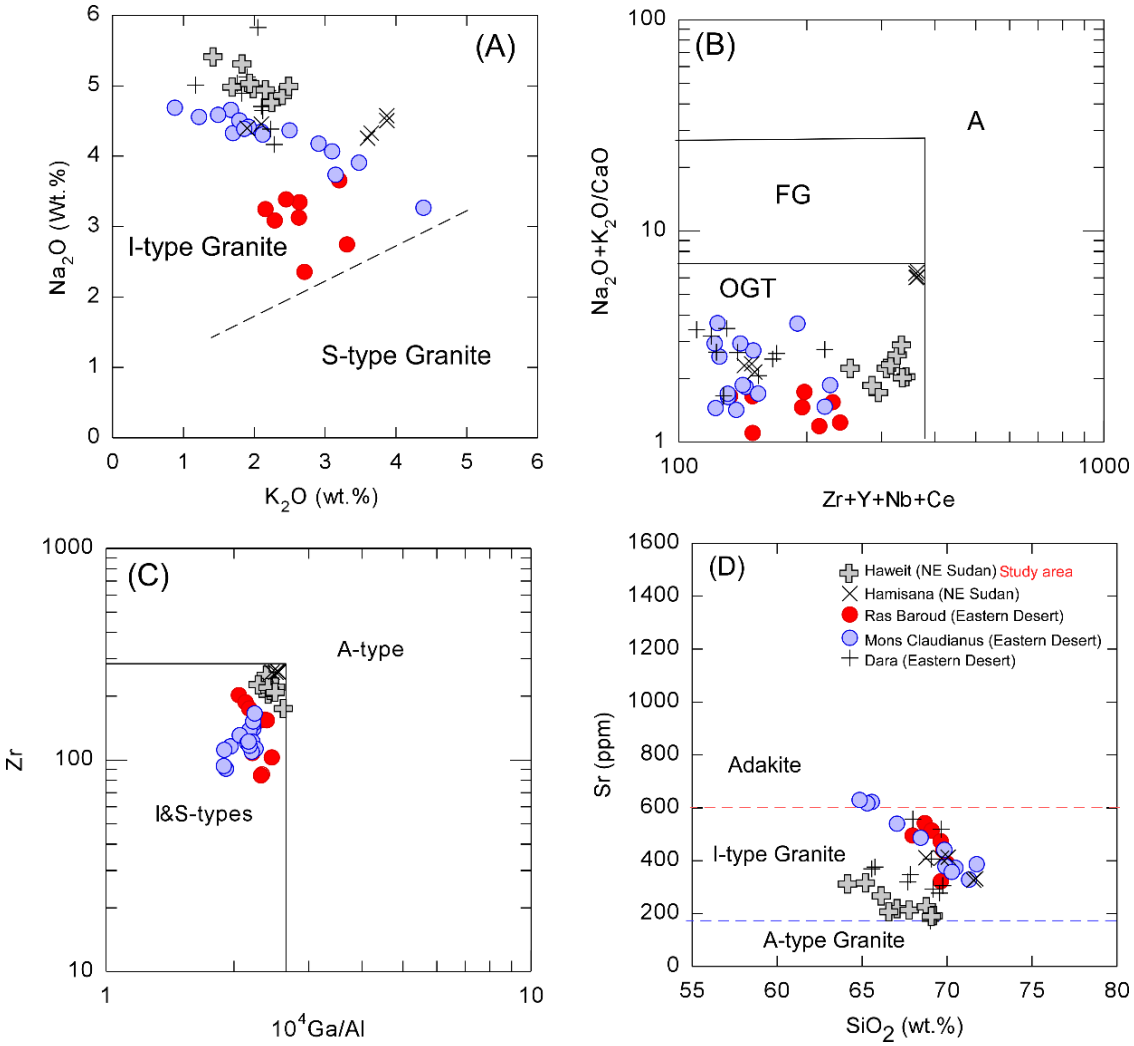

Figure 9. (**A**) K_2O vs. Na_2O diagram [56]; (**B**) $(K_2O + Na_2O)/CaO$ vs. (Zr + Nb + Ce + Y) and (**C**) Zr (ppm) vs. 10000Ga/Al diagrams of the Haweit granodiorites [57], where A = A-type granite; FG = M + I + S-type fractional granite; OGT = non-fractional M + I + S-type granite; and (**D**) Sr vs. SiO_2 diagram where the A-type, I-type, and adakite division is after Su et al. [58]. The data of other granodiorite samples from various localities in the Nubian Shield, including Hamisana [13], Ras Baroud [41], Mons Claudianus [42], and Dara [43], are used for comparison.

Their metaluminous nature and the noticeably low P_2O_5 concentrations (0.17–0.33 wt.%) confirm their I-type affinity and rule out the possibility of belonging to S-type granites, which in general are strongly peraluminous with high P_2O_5 concen-

trations. Moreover, using the relation between (Na_2O + K_2O)/CaO vs. Zr + Ce + Nb + Y and Zr vs. 10,000 × Ga/Al plots (Figure 9B,C), the samples belong to unfractionated I-type granites [57], similar to granodiorites from other localities over the Nubian Shield. Furthermore, the low Zr content (172–249 ppm) and moderate Sr content (191–318 ppm) of the investigated granites indicate that they are most likely I-type granites, rather than adakite or A-type granites (Figure 9D). Accordingly, the Haweit granodiorites are typical calc-alkaline I-type granites.

5.3. Magma Source and Petrogenesis

The origin and genesis of calc-alkaline I-type granites is still a debated topic. In general, they could be generated by (1) differentiation of mantle-derived mafic melts [59]; (2) mixing of mafic and felsic melts [5]; and (3) variable degrees of partial melting from a mafic sources [60]. When compared to typical mantle-derived intermediate rocks, the Haweit granodiorites have higher Na_2O (4.76–5.41 wt.%) and lower MgO (0.57–1.31 wt.%) values, with Mg# (19.5–34.4), Cr (4.12–6.70 ppm), and V (20.04–29.25 ppm) contents, implying that the mantle-derived intermediate source is unreasonable [61]. The magma mixing would result in the formation of mafic enclaves and then changes in the geochemical characteristics [5]. Geochemically, the studied granodiorites show narrow geochemical variations; this is beside the entirely absence of mafic microgranular enclaves in the pluton which argue against a magma mixing scenario. In the SiO_2 vs. Mg# diagram (Figure 10A), where reference fields represent experimentally dehydration melting data of different sources under crustal P (0.5–1.5 GPa) and (800–1000 °C) values, the Haweit granodiorites do not fit the magma mixing trend, implying that they were not generated through the magma mixing process.

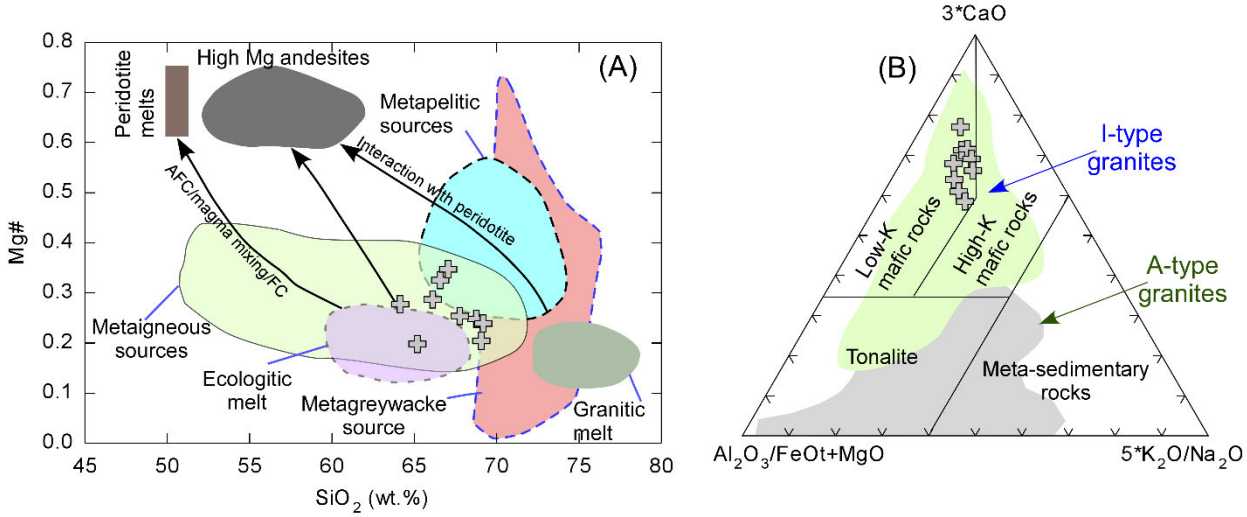

Figure 10. (**A**) SiO_2 versus Mg# diagram (reference fields represent experimentally dehydration melting data of different sources under crustal P (0.5–1.5 GPa) and (800–1000 °C) values after Patiño Douce, [62]; Wolf and Wyllie, [63]); and (**B**) Ternary diagram of $Al_2O_3/(FeO^t + MgO) - 3*CaO - 5*(K_2O/Na_2O)$ [64], showing that the Haweit granodiorite were likely derived from a low-K mafic magma source. The fields of A-type and I-type granites from the ANS are adopted from Robinson et al. [65,66].

Calc-alkaline I-type granitic magma could be created if the mafic rocks are partially melted [63]. The analyzed zircons clearly show a narrow range in εHf(t) (+7.34 to +11.21) between the depleted mantle (DM) and chondritic uniform reservoir (CHUR), implying that the calc-alkaline granitic magmas might be generated from juvenile components [52]. The Haweit granodiorites were mostly formed from Neoproterozoic juvenile lower mafic crustal materials, as evidenced by the high positive zircon εHf(t) values (+7.34 to +11.21) (Figure 7) and crustal Hf model ages of 734–985 Ma (Figure 8). Their low Rb/Y (1.78–3.71)

and Nb/Y (0.17–0.56) ratios also refer to a lower mafic crust source [67]. Moreover, the low K_2O concentrations are compatible with their genesis from a mafic source. Using Laurent et al.'s [64] ternary discrimination diagram (Figure 10B), where fields were experimentally detected based on the major elements composition of melts originated from various source rocks, samples are plotted in the field of melts derived from low-K mafic rocks. Therefore, a low-K mafic lower crust source is preferred for the Haweit granodiorites.

The granodioritic metaluminous melts could be experimentally generated by amphibolites dehydration melting within the lower crust [68]. The high Yb (3.29–6.11 ppm) and Y (14–46 ppm) contents may indicate that the source rocks were situated at the amphibole stability field. However, the depletion of HFSEs (e.g., Nb, Ta, and Hf) (Figure 6A) inherit from their source rocks rather than amphibole fractionation [69]. We suggest that the protolith of the Haweit granodiorites was probably derived from the partial melting of a lower crustal mafic source. The binary relation between $(La)_N$ vs. $(La/Sm)_N$ and also Th vs. Th/Nd ratios (Figure 11 A,B) is further evidence that partial melting is the main magmatic mechanism responsible for the formation of the studied granodiorites and that the fractionation of some minerals in the melting residue has a minor impact on changes in the elemental ratios. Zircon U-Pb analysis (Figure 3, Table 1) and high εHf(t) values (+7.34 to +11.21) also support the formation of granodiorites by partial melting of the mafic crust that might have been geochemically influenced by subduction.

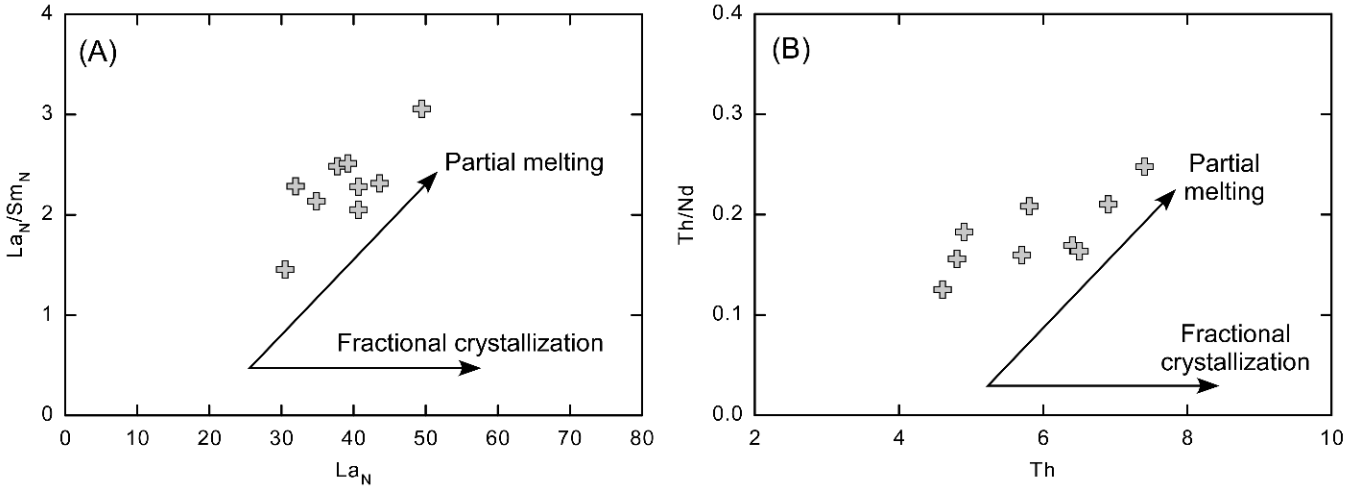

Figure 11. Binary relation between $(La)_N$ vs. $(La/Sm)_N$ (**A**) and Th vs. Th/Nd (**B**), showing that partial melting is the major magmatic process to control the formation of the Haweit granodiorites.

5.4. Tectonic Setting Implication

The tectonic evolution of the ANS crust through the interval time of 900–740 Ma was characterized by the development of juvenile crust [29]. The ANS was developed via five main tectonic events, including continental rifting (~900–860 Ma), oceanic spreading (~860–830 Ma), the formation of oceanic arcs and cogenetic basins due to subduction (~830–700 Ma), island arcs accretion (~750–650 Ma), and late to post-collisional magmatism (~ 640–550 Ma) [70]. These tectonic events were established based on precious isotopic data, including Rb-Sr and zircon U-Pb, from many localities in the ANS [27]. However, the Sudanese part of the Nubian Shield, especially the Gabgaba Terrane, still needs further investigation to contribute to the tectonic evolution of the ANS. The new zircon U-Pb and Lu-Hf isotope data are critically valuable for understanding the tectonic evolution of the Haweit granodiorites in NE Sudan, as well as the regional development of the middle part of the Nubian Shield.

The Haweit granodiorites were emplaced during the Cryogenian (ca. 719 Ma) within the framework of the Gabgaba Terrane's island arc magmatism (NE Sudan). The Neoproterozoic magmatism in the study area encompasses, along with granitic rocks, other older Tonian intermediate (andesites; ca. 752 Ma) to mafic (basaltic andesites; ca. 773 Ma) vol-

canics [25]. The Haweit granodiorites have a typical subduction-related magma signature, as inferred from their metaluminous composition and relative depletion in HFSEs relative to LILEs with an apparent negative Nb anomaly (Figure 6). The isotopic data also suggest the intrusion of Haweit granodiorites in the subduction-related tectono-magmatism. The Haweit granodiorite (718.5 ± 2 Ma) was emplaced chronologically with syn-collisional granodiorites (e.g., Gabal Dara; 720 Ma) in the Eastern Desert [43] on the northern side of the Nubian Shield. This indicates that Haweit granodioritic magma was generated during the early magmatic/tectonic stages of the ANS (765–610 Ma; [71]).

The studied granodiorites have typical arc setting characteristics as exhibited by the negative Nb, Ta, and Ti anomalies and the slightly positive U and Ba anomalies (Figure 6A). The discrimination diagrams for Rb vs. Yb + Ta and Y vs. Nb suggest a volcanic arc environment for the Haweit granodiorites (Figure 12A,B), similar to other chronologically granodiorites from several localities over the Nubian Shield. The VAG tectonic setting, along with the enrichment of granodiorites with LILEs over HFSEs and clear negative Nb anomalies (Figure 6A), suggest the involvement of the metasomatized lithospheric mantle due to subduction-related processes in the generation of Haweit granodiorites magma. The role of the lithospheric mantle in the genesis of VAG granitic magmas in NE Sudan and other comparable varieties in the Egyptian Eastern Desert and Sinai is widely accepted due to the ability of the lithospheric mantle to preserve the geochemical characteristics of subduction [43].

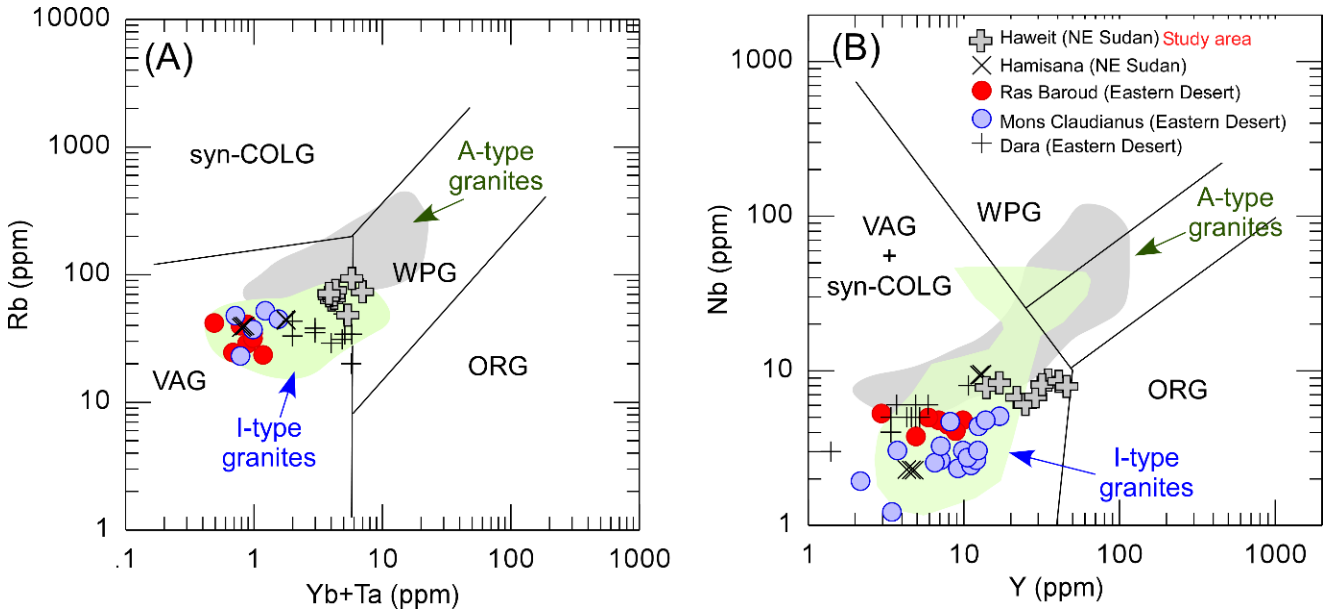

Figure 12. (**A**) Rb vs. Y + Ta [72] and (**B**) Nb vs. Y [73] tectonic discrimination diagrams for the Haweit granodiorite. VAG: volcanic arc granites; ORG: ocean ridge granites; WPG: within plate granites; syn-COLG: syn-collision granites. The fields of A-type and I-type granites from the ANS are adopted from Robinson et al. [65,66].

The integration of new data reported in this work with earlier research results can help in tracking the tectonic evolution of the Gabgaba Terrane throughout Neoproterozoic (Figure 13). Accordingly, based on the presented data, we suggest that the Haweit granodioritic pluton may be formed due to the subduction of the oceanic crust (Figure 13). Due to subduction, a mafic arc crust was created because of the partial melting of the mantle wedge. The mantle wedge was metasomatized by the subduction slab components (fluids or melts). Following this, the modified mantle wedge partially melted, and the mantle-derived magmas upwelled. As a result, these mantle-derived magmas accumulated at different levels through the crust and underwent a strong differentiation to form the older mafic rocks (ca. 752–773 Ma; [25]) in the Gabgaba terrane (NE Sudan). Subsequently, at ca. 719 Ma,

the upwelling of the asthenosphere heated and partially melted the pre-existing lower crust mafic materials to produce the Haweit granodioritic magma in Gabgaba Terrane, NE Sudan.

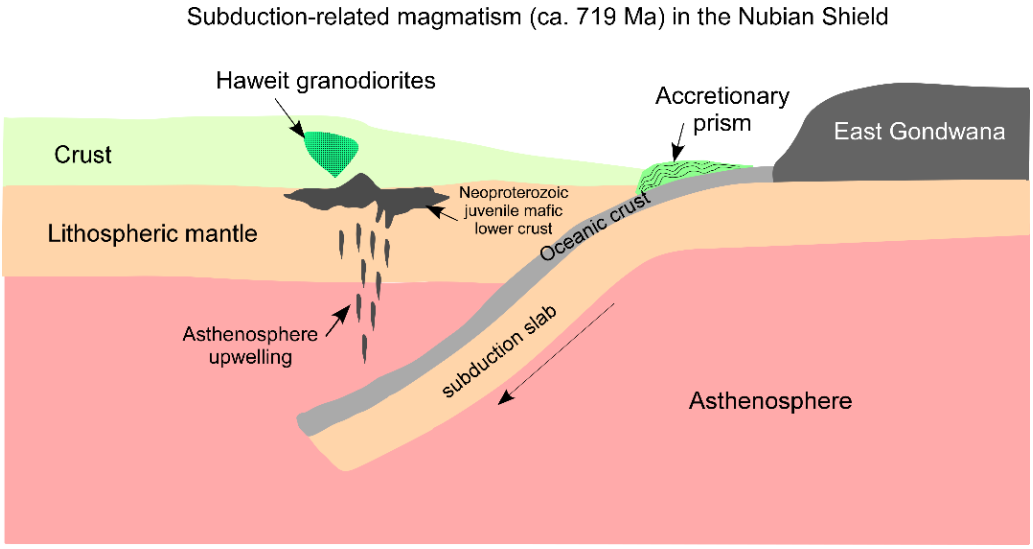

Figure 13. A sketch model shows the subduction tectonic evolution (ca. 719 Ma) of the Haweit granodiorites in Gabgaba Terrane, NE Sudan. Not to scale.

6. Conclusions

Zircon U–Pb dating indicates that the Haweit granodiorites were crystallized during the Cryogenian (718.5 ± 2.2 Ma). The Haweit granodiorites are calc-alkaline rocks with a typical subduction-related setting signature. Moreover, they are rich in Na_2O and have a metaluminous nature. Their mineralogical and geochemical characters indicate that they belong to the I-type granites. The in situ zircon Hf isotopic data suggest that granodiorites have a juvenile crust character and were originated from a depleted mantle source with no contribution from pre-Neoproterozoic crustal materials. The granodiorites were essentially formed by the partial melting of the Neoproterozoic juvenile mafic lower crust. They formed due to subduction, where asthenosphere upwelling is the main tectono-magmatic process responsible for the melting of the lower mafic crust and the formation of the Haweit granodiorites in Gabgaba Terrane, NE Sudan.

Supplementary Materials: Analytical Methods. The following supporting information can be downloaded at: https://www.mdpi.com/article/10.3390/min13030331/s1.

Author Contributions: Conceptualization, M.S. and S.A.; methodology, M.M.A.A., X.L. and S.S.A.; software, M.S., E.S.R.L., D.F. and E.S.F.; validation, N.M.M., A.R.A.A.R. and A.S.; formal analysis, M.M.A.A. and X.L.; investigation, H.M.H.Z. and A.E.; resources, M.M.A.A., A.R.A.A.R. and A.S; data curation, M.S. and N.M.M.; writing—original draft preparation, M.S., M.M.A.A., D.F. and S.A.; writing—review and editing, M.S., H.M.H.Z., E.S.R.L. and S.A.; visualization, S.S.A.; supervision, H.M.H.Z. and X.L.; project administration, M.M.A.A. and X.L.; funding acquisition, A.E. and S.S.A. All authors have read and agreed to the published version of the manuscript.

Funding: This research was supported by Researchers Supporting Project number (RSP2023R496), King Saud University, Riyadh, Saudi Arabia. The author AE would like to thank "Dunarea de Jos" University of Galati, Romania, INPOLDE infrastructure, for the material and technical support.

Data Availability Statement: Not applicable.

Acknowledgments: This research was supported by Researchers Supporting Project number (RSP2023R496), King Saud University, Riyadh, Saudi Arabia. The author A.E. would like to thank "Dunarea de Jos" University of Galati, Romania, INPOLDE infrastructure, for the material and technical support. The authors would like to thank the editors and the reviewers for their precious time, detailed and constructive reviews, and additional comments which significantly improved the manuscript.

Conflicts of Interest: The authors declare no conflict of interest.

References

1. Robinson, F.A.; Foden, J.D.; Collins, A.S. Geochemical and isotopic constraints on island arc, synorogenic, post-orogenic and anorogenic granitoids in the Arabian Shield, Saudi Arabia. *Lithos* **2015**, *220–223*, 97–115. [CrossRef]
2. Zhou, G.; Wu, Y.; Wang, H.; Qin, Z.; Zhang, W.; Zheng, J.; Yang, S. Petrogenesis of the Huashanguan A-type granite complex and its implications for the early evolution of the Yangtze Block. *Precambrian Res.* **2017**, *292*, 57–74. [CrossRef]
3. Gamal El Dien, H.; Li, Z.-X.; Abu Anbar, M.; Doucet, L.S.; Murphy, J.B.; Evans, N.J.; Xia, X.-P.; Li, J. The largest plagiogranite on Earth formed by re-melting of juvenile proto-continental crust. *Commun. Earth Environ.* **2021**, *2*, 138. [CrossRef]
4. Sami, M.; El Monsef, M.A.; Abart, R.; Toksoy-Köksal, F.; Abdelfadil, K.M. Unraveling the Genesis of Highly Fractionated Rare-Metal Granites in the Nubian Shield via the Rare-Earth Elements Tetrad Effect, Sr–Nd Isotope Systematics, and Mineral Chemistry. *ACS Earth Space Chem.* **2022**, *6*, 2368–2384. [CrossRef]
5. Kemp, A.I.S.; Hawkesworth, C.J.; Foster, G.L.; Paterson, B.A.; Woodhead, J.D.; Hergt, J.M.; Gray, C.M.; Whitehouse, M.J. Magmatic and Crustal Differentiation History of Granitic Rocks from Hf-O Isotopes in Zircon. *Science* **2007**, *315*, 980–983. [CrossRef] [PubMed]
6. Chappell, B.W.; Bryant, C.J.; Wyborn, D. Peraluminous I-type granites. *Lithos* **2012**, *153*, 142–153. [CrossRef]
7. Weidendorfer, D.; Mattsson, H.B.; Ulmer, P. Dynamics of magma mixing in partially crystallized magma chambers: Textural and petrological constraints from the basal complex of the Austurhorn intrusion (SE Iceland). *J. Petrol.* **2014**, *55*, 1865–1903. [CrossRef]
8. Clemens, J.D. Granitic magmas with I-type affinities, from mainly metasedimentary sources: The Harcourt batholith of southeastern Australia. *Contrib. Mineral. Petrol.* **2018**, *173*, 93. [CrossRef]
9. Barbarin, B. Mafic magmatic enclaves and mafic rocks associated with some granitoids of the central Sierra Nevada batholith, California: Nature, origin, and relations with the hosts. *Lithos* **2005**, *80*, 155–177. [CrossRef]
10. Clemens, J.; Stevens, G. What controls chemical variation in granitic magmas? *Lithos* **2012**, *134*, 317–329. [CrossRef]
11. Zhu, R.-Z.; Lai, S.-C.; Qin, J.-F.; Zhao, S.-W. Petrogenesis of late Paleozoic-to-early Mesozoic granitoids and metagabbroic rocks of the Tengchong Block, SW China: Implications for the evolution of the eastern Paleo-Tethys. *Int. J. Earth Sci.* **2018**, *107*, 431–457. [CrossRef]
12. Meert, J.G.; Lieberman, B.S. The Neoproterozoic assembly of Gondwana and its relationship to the Ediacaran–Cambrian radiation. *Gondwana Res.* **2008**, *14*, 5–21. [CrossRef]
13. Saeed, A.; Zeng, Z.; Dilek, Y.; Awadelseid, S.F.; Abdel Rahman, A.A.; Adam, M.M.A. Geochronology, geochemistry, and Hf–Sr-Nd isotopes of the Hamisana Shear Zone granitoids in northeastern Sudan: Petrogenesis and tectonic evolution of neoproterozoic juvenile crust in the Nubian Shield. *Precambrian Res.* **2020**, *347*, 105857. [CrossRef]
14. Lasheen, E.S.R.; Saleh, G.M.; Khaleal, F.M.; Alwetaishi, M. Petrogenesis of neoproterozoic ultramafic rocks, Wadi Ibib–Wadi Shani, South Eastern Desert, Egypt: Constraints from whole rock and mineral chemistry. *Appl. Sci.* **2021**, *11*, 10524. [CrossRef]
15. Johnson, P.R.; Woldehaimanot, B. Development of the Arabian-Nubian Shield: Perspectives on accretion and deformation in the northern East African Orogen and the assembly of Gondwana. *Geol. Soc. Lond. Spec. Publ.* **2003**, *206*, 289–325. [CrossRef]
16. Stern, R.J.; Nielsen, K.C.; Best, E.; Sultan, M.; Arvidson, R.E.; Kröner, A. Orientation of late Precambrian sutures in the Arabian-Nubian shield. *Geology* **1990**, *18*, 1103–1106. [CrossRef]
17. Ali, S.; Ntaflos, T.; Sami, M. Geochemistry of Khor Um-Safi ophiolitic serpentinites, central Eastern desert, Egypt: Implications for neoproterozoic arc-basin system in the Arabian-Nubian shield. *Geochemistry* **2021**, *81*, 125690. [CrossRef]
18. Ali, S.; Abart, R.; Sayyed, M.I.; Hauzenberger, C.A.; Sami, M. Petrogenesis of the Wadi El-Faliq Gabbroic Intrusion in the Central Eastern Desert of Egypt: Implications for Neoproterozoic Post-Collisional Magmatism Associated with the Najd Fault System. *Minerals* **2023**, *13*, 10. [CrossRef]
19. Hamdy, M.M.; Lasheen, E.S.R.; Abdelwahab, W. Gold-bearing listwaenites in ophiolitic ultramafics from the Eastern Desert of Egypt: Subduction zone-related alteration of Neoproterozoic mantle? *J. Afr. Earth Sci.* **2022**, *193*, 104574. [CrossRef]
20. Abdelfadil, K.M.; Saleh, G.M.; Putiš, M.; Sami, M. Mantle source characteristics of the late Neoproterozoic post-collisional gabbroic intrusion of Wadi Abu Hadieda, north Arabian-Nubian Shield, Egypt. *J. Afr. Earth Sci.* **2022**, *194*, 104607. [CrossRef]
21. Abd El Monsef, M.; Sami, M.; Toksoy-Köksal, F.; Abart, R.; Ondrejka, M.; Abdelfadil, K.M. Role of Magmatism and Related-Exsolved Fluids during Ta-Nb-Sn Concentration in the Central Eastern Desert of Egypt: Evidences from Mineral Chemistry and Fluid Inclusions. *J. Earth Sci.* **2023**. [CrossRef]
22. Sami, M.; Azer, M.; Abdel-Karim, A.-A. Post-collisional Ferani volcanics from north Arabian-Nubian Shield (south Sinai, Egypt): Petrogenesis and implication for Ediacaran (607-593 Ma) geodynamic evolution. *J. Geol.* **2023**. [CrossRef]

23. Abu-Fatima, M.; Marignac, C.; Cathelineau, M.; Boiron, M.C. Metallogeny of a Pan-African oceanic arc: VHMS and gold deposits in the Ariab-Arbaat belt, Haya terrane, Red Sea Hills (Sudan). *Gondwana Res.* **2021**, *98*, 76–106. [CrossRef]
24. Adam, M.M.A.; Lv, X.; Abdel Rahman, A.A.; Stern, R.J.; Abdalrhman, A.A.A.; Ullah, Z. In-situ sulfur isotope and trace element compositions of pyrite from the Neoproterozoic Haweit gold deposit, NE Sudan: Implications for the origin and source of the sulfur. *Ore Geol. Rev.* **2020**, *120*, 103405. [CrossRef]
25. Adam, M.M.A.; Lv, X.; Fathy, D.; Abdel Rahman, A.R.A.; Ali, A.A.; Mohammed, A.S.; Farahat, E.S.; Sami, M. Petrogenesis and tectonic implications of Tonian island arc volcanic rocks from the Gabgaba Terrane in the Arabian-Nubian Shield (NE Sudan). *J. Asian Earth Sci.* **2022**, *223*, 105006. [CrossRef]
26. Bierlein, F.P.; McKeag, S.; Reynolds, N.; Bargmann, C.J.; Bullen, W.; Murphy, F.C.; Al-Athbah, H.; Brauhart, C.; Potma, W.; Meffre, S.; et al. The Jebel Ohier deposit—A newly discovered porphyry copper–gold system in the Neoproterozoic Arabian–Nubian Shield, Red Sea Hills, NE Sudan. *Miner. Depos.* **2016**, *51*, 713–724. [CrossRef]
27. Gamaleldien, H.; Li, Z.-X.; Anbar, M.A.; Murphy, J.B.; Evans, N.J.; Xia, X.-P. Formation of juvenile continental crust in northern Nubian Shield: New evidence from granitic zircon U-Pb-Hf-O isotopes. *Precambrian Res.* **2022**, *379*, 106791. [CrossRef]
28. Abdelsalam, M.G.; Stern, R.J. Sutures and shear zones in the Arabian-Nubian Shield. *J. Afr. Earth Sci.* **1996**, *23*, 289–310. [CrossRef]
29. Stern, R.J.; Abdelsalam, M.G. Formation of juvenile continental crust in the Arabian–Nubian shield: Evidence from granitic rocks of the Nakasib suture, NE Sudan. *Geol. Rundsch.* **1998**, *87*, 150–160. [CrossRef]
30. Abdel-Karim, A.-A.; Azer, M.; Sami, M. Petrogenesis and tectonic implications of the Maladob ring complex in the South Eastern Desert, Egypt: New insights from mineral chemistry and whole-rock geochemistry. *Int. J. Earth Sci.* **2020**, *110*, 53–80. [CrossRef]
31. Lasheen, E.S.R.; Mohamed, W.H.; Ene, A.; Awad, H.A.; Azer, M.K. Implementation of petrographical and aeromagnetic data to determine depth and structural trend of homrit waggat area, central Eastern Desert, Egypt. *Appl. Sci.* **2022**, *12*, 8782. [CrossRef]
32. Kröner, A.; Greiling, R.; Reischmann, T.; Hussein, I.; Stern, R.; Dürr, S.; Krüger, J.; Zimmer, M. Pan-African crustal evolution in the Nubian segment of northeast Africa. *Proterozic Lithospheric Evol.* **1987**, *17*, 235–257.
33. Stern, R.J.; Kroner, A.; Manton, W.I.; Reischmann, T.; Mansour, M.; Hussein, I.M. Geochronology of the Late Precambrian Hamisana Shear Zone, Red-Sea Hills, Sudan and Egypt. *J. Geol. Soc.* **1989**, *146*, 1017–1029. [CrossRef]
34. El-Nisr, S.A. Late Precambrian volcanism at Wadi Allaqi, south Eastern Desert, Egypt: Evidence for transitional continental arc/margin environment. *J. Afr. Earth Sci.* **1997**, *24*, 301–313. [CrossRef]
35. Lissan, N.H.; Bakheit, A.K. The Geology and Geochemistry of Metavolcanic Rocks from Artoli Area, Berber Province, Northern Sudan: An Implication for Petrogenetic and Tectonic Setting. *J. Am. Sci.* **2010**, *6*, 1–13.
36. Hoskin, P.W.O.; Schaltegger, U. The composition of zircon and igneous and metamorphic petrogenesis. *Rev. Mineral. Geochem.* **2003**, *53*, 27–62. [CrossRef]
37. Middlemost, E.A.K. Naming materials in the magma/igneous rock system. *Earth-Sci. Rev.* **1994**, *37*, 215–224. [CrossRef]
38. Irvine, T.N.; Baragar, W.R.A. A Guide to the Chemical Classification of the Common Volcanic Rocks. *Can. J. Earth Sci.* **1971**, *8*, 523–548. [CrossRef]
39. Roberts, M.P.; Clemens, J.D. Origin of high-potassium, calc-alkaline, I-type granitoids. *Geology* **1993**, *21*, 825–828. [CrossRef]
40. Frost, B.R.; Barnes, C.G.; Collins, W.J.; Arculus, R.J.; Ellis, D.J.; Frost, C.D. A geochemical classification for granitic rocks. *J. Petrol.* **2001**, *42*, 2033–2048. [CrossRef]
41. El-Bialy, M.Z.; Omar, M.M. Spatial association of Neoproterozoic continental arc I-type and post-collision A-type granitoids in the Arabian–Nubian Shield: The Wadi Al-Baroud Older and Younger Granites, North Eastern Desert, Egypt. *J. Afr. Earth Sci.* **2015**, *103*, 1–29. [CrossRef]
42. Abdel-Rahman, A.-F.M. Geochemistry, age and origin of the Mons Claudianus TTG batholith (Egypt): Insight into the role of Pan-African magmatism in uniting plates of Gondwana. *Geol. Mag.* **2018**, *156*, 969–988. [CrossRef]
43. Eliwa, H.A.; Breitkreuz, C.; Murata, M.; Khalaf, I.M.; Bulhler, B.; Itaya, T.; Takahashi, T.; Hirahara, Y.; Miyazaki, T.; Kimura, J.I.; et al. SIMS zircon U-Pb and mica K-Ar geochronology, and Sr-Nd isotope geochemistry of Neoproterozoic granitoids and their bearing on the evolution of the north Eastern Desert, Egypt. *Gondwana Res.* **2014**, *25*, 1570–1598. [CrossRef]
44. Sun, S.-S.; McDonough, W.F. Chemical and isotopic systematics of oceanic basalts: Implications for mantle composition and processes. *Geol. Soc. Lond. Spec. Publ.* **1989**, *42*, 313–345. [CrossRef]
45. Moyen, J.-F. The composite Archaean grey gneisses: Petrological significance, and evidence for a non-unique tectonic setting for Archaean crustal growth. *Lithos* **2011**, *123*, 21–36. [CrossRef]
46. Scherer, E.E.; Cameron, K.L.; Blichert-Toft, J. Lu–hf garnet geochronology: Closure temperature relative to the Sm–Nd system and the effects of trace mineral inclusions. *Geochim. Cosmochim. Acta* **2000**, *64*, 3413–3432. [CrossRef]
47. Kinny, P.D.; Maas, R. Lu-Hf and Sm-Nd isotope systems in zircon. *Rev. Mineral. Geochem.* **2003**, *53*, 327–341. [CrossRef]
48. Spencer, C.J.; Kirkland, C.L.; Roberts, N.M.W.; Evans, N.J.; Liebmann, J. Strategies towards robust interpretations of in situ zircon Lu–Hf isotope analyses. *Geosci. Front.* **2020**, *11*, 843–853. [CrossRef]
49. Hiess, J.; Bennett, V.C.; Nutman, A.P.; Williams, I.S. In situ U–Pb, O and Hf isotopic compositions of zircon and olivine from Eoarchaean rocks, West Greenland: New insights to making old crust. *Geochim. Cosmochim. Acta* **2009**, *73*, 4489–4516. [CrossRef]
50. Ali, K.A.; Kroner, A.; Hegner, E.; Wong, J.; Li, S.Q.; Gahlan, H.A.; Abu El Ela, F.F. U-Pb zircon geochronology and Hf-Nd isotopic systematics of Wadi Beitan granitoid gneisses, South Eastern Desert, Egypt. *Gondwana Res.* **2015**, *27*, 811–824. [CrossRef]
51. Belousova, E.A.; Griffin, W.L.; O'Reilly, S.Y. Zircon Crystal Morphology, Trace Element Signatures and Hf Isotope Composition as a Tool for Petrogenetic Modelling: Examples From Eastern Australian Granitoids. *J. Petrol.* **2006**, *47*, 329–353. [CrossRef]

52. Griffin, W.L.; Wang, X.; Jackson, S.E.; Pearson, N.J.; O'Reilly, S.Y.; Xu, X.; Zhou, X. Zircon chemistry and magma mixing, SE China: In-situ analysis of Hf isotopes, Tonglu and Pingtan igneous complexes. *Lithos* **2002**, *61*, 237–269. [CrossRef]
53. Hargrove, U.S.; Stern, R.J.; Kimura, J.I.; Manton, W.I.; Johnson, P.R. How juvenile is the Arabian–Nubian Shield? Evidence from Nd isotopes and pre-Neoproterozoic inherited zircon in the Bi'r Umq suture zone, Saudi Arabia. *Earth Planet. Sci. Lett.* **2006**, *252*, 308–326. [CrossRef]
54. Zheng, J.; Griffin, W.L.; O'Reilly, S.Y.; Lu, F.; Wang, C.; Zhang, M.; Wang, F.; Li, H. 3.6 Ga lower crust in central China: New evidence on the assembly of the North China craton. *Geology* **2004**, *32*, 229–232. [CrossRef]
55. Collins, W.J.; Huang, H.-Q.; Bowden, P.; Kemp, A.I.S. Repeated S–I–A-type granite trilogy in the Lachlan Orogen and geochemical contrasts with A-type granites in Nigeria: Implications for petrogenesis and tectonic discrimination. *Geol. Soc. Lond. Spec. Publ.* **2020**, *491*, 53–76. [CrossRef]
56. Chappell, B.W.; White, A.J.R.; Brown, P.E.; Chappell, B.W. I- and S-type granites in the Lachlan Fold Belt. In *The Second Hutton Symposium on the Origin of Granites and Related Rocks*; Geological Society of America: Boulder, CO, USA, 1992; Volume 272.
57. Whalen, J.B.; Currie, K.L.; Chappell, B.W. A-type granites: Geochemical characteristics, discrimination and petrogenesis. *Contrib. Mineral. Petrol.* **1987**, *95*, 407–419. [CrossRef]
58. Su, Y.; Zheng, J.; Griffin, W.L.; Zhao, J.; Suzanne, Y.; Tang, H.; Ping, X.; Xiong, Q. Petrogenesis and geochronology of Cretaceous adakitic, I-and A-type granitoids in the NE Yangtze block: Constraints on the eastern subsurface boundary between the North and South China blocks. *Lithos* **2013**, *175*, 333–350. [CrossRef]
59. Soesoo, A. Fractional crystallization of mantle-derived melts as a mechanism for some I-type granite petrogenesis: An example from Lachlan Fold Belt, Australia. *J. Geol. Soc.* **2000**, *157*, 135–149. [CrossRef]
60. Clemens, J.D.; Darbyshire, D.P.F.; Flinders, J. Sources of post-orogenic calcalkaline magmas: The Arrochar and Garabal Hill–Glen Fyne complexes, Scotland. *Lithos* **2009**, *112*, 524–542. [CrossRef]
61. Smithies, R.; Champion, D. The Archaean high-Mg diorite suite: Links to tonalite–trondhjemite–granodiorite magmatism and implications for early Archaean crustal growth. *J. Petrol.* **2000**, *41*, 1653–1671. [CrossRef]
62. Patiño Douce, A.E. What do experiments tell us about the relative contributions of crust and mantle to the origin of granitic magmas? *Geol. Soc. Lond. Spec. Publ.* **1999**, *168*, 55–75. [CrossRef]
63. Wolf, M.B.; Wyllie, P.J. Dehydration-melting of amphibolite at 10 kbar: The effects of temperature and time. *Contrib. Mineral. Petrol.* **1994**, *115*, 369–383. [CrossRef]
64. Laurent, O.; Martin, H.; Moyen, J.F.; Doucelance, R. The diversity and evolution of late-Archean granitoids: Evidence for the onset of "modern-style" plate tectonics between 3.0 and 2.5Ga. *Lithos* **2014**, *205*, 208–235. [CrossRef]
65. Robinson, F.A.; Foden, J.D.; Collins, A.S.; Payne, J.L. Arabian Shield magmatic cycles and their relationship with Gondwana assembly: Insights from zircon U-Pb and Hf isotopes. *Earth Planet. Sci. Lett.* **2014**, *408*, 207–225. [CrossRef]
66. Robinson, F.A.; Bonin, B.; Pease, V.; Anderson, J. A discussion on the tectonic implications of Ediacaran late-to post-orogenic A-type granite in the northeastern Arabian Shield, Saudi Arabia. *Tectonics* **2017**, *36*, 582–600. [CrossRef]
67. Rudnick, R.L.; Fountain, D.M. Nature and composition of the continental crust: A lower crustal perspective. *Rev. Geophys.* **1995**, *33*, 267–309. [CrossRef]
68. Beard, J.S.; Lofgren, G.E. Dehydration melting and water-saturated melting of basaltic and andesitic greenstones and amphibolites at 1, 3, and 6. 9 kb. *J. Petrol.* **1991**, *32*, 365–401. [CrossRef]
69. Zhao, S.-w.; Lai, S.-c.; Qin, J.-f.; Zhu, R.-Z.; Wang, J.-b. Geochemical and geochronological characteristics of Late Cretaceous to Early Paleocene granitoids in the Tengchong Block, Southwestern China: Implications for crustal anatexis and thickness variations along the eastern Neo-Tethys subduction zone. *Tectonophysics* **2017**, *694*, 87–100. [CrossRef]
70. Fritz, H.; Abdelsalam, M.; Ali, K.A.; Bingen, B.; Collins, A.S.; Fowler, A.R.; Ghebreab, W.; Hauzenberger, C.A.; Johnson, P.R.; Kusky, T.M.; et al. Orogen styles in the East African Orogen: A review of the Neoproterozoic to Cambrian tectonic evolution. *J. Afr. Earth Sci.* **2013**, *86*, 65–106. [CrossRef]
71. Stern, R.J.; Hedge, C.E. Geochronologic and isotopic constraints on late Precambrian crustal evolution in the Eastern Desert of Egypt. *Am. J. Sci.* **1985**, *285*, 97–127. [CrossRef]
72. Pearce, J.A.; Harris, N.B.W.; Tindle, A.G. Trace Element Discrimination Diagrams for the Tectonic Interpretation of Granitic Rocks. *J. Petrol.* **1984**, *25*, 956–983. [CrossRef]
73. Pearce, J.A. Sources and settings of granitic rocks. *Episodes* **1996**, *19*, 120–125. [CrossRef]